# Elucidation of Amyloid-Beta's Gambit in Oligomerization:

# Truncated Aβ fragments of residues Aβ1-23, Aβ1-24 and Aβ1-25 rapidly seed to form SDS-stable, LMW Aβ oligomers that impair synaptic plasticity.

**Beatriz Gil[1+], Jamie Rose[2+], Davide Demurtas[3], Gian-Filippo Mancini[4], Jessica Sordet-Dessimoz[4], Vincenzo Sorrentino[5], Nikita Rudinskiy[6], Matthew P. Frosch[7], Bradley T. Hyman[6], Marc Moniatte[8], Tara. L. Spires-Jones[2], Caroline E. Herron[1] and Adrien W. Schmid[8*].**

[1]Conway Institute of Biomolecular and Biomedical Research, University College of Dublin (UCD), Ireland.
[2]UK Dementia Research Institute and Centre for Discovery Brain Sciences at The University of Edinburgh, Edinburgh, Scotland.
[3]Interdisciplinary Centre for Electron Microscopy (CIME), EPFL, Switzerland.
[4]Histology Core Facility, Ecole Polytechnique Fédérale de Lausanne (EPFL), Switzerland.
[5] Healthy Longevity Translational Research Programme, Yong Loo Lin School of Medicine & Department of Biochemistry, National University of Singapore.
[6]Harvard Medical School, Mass General Hospital, Massachusetts Boston, USA
[7]Massachusetts General Hospital and Harvard Medical School, Massachusetts General Institute for Neurodegenerative Disease, Charlestown, MA, USA.
[8]Proteomics Core Facility, Ecole Polytechnique Fédérale de Lausanne (EPFL), Lausanne, Switzerland.
[+] Contributed equally

*To whom correspondence should be addressed:

Adrien W. Schmid, PhD.
Life Sciences (SV), PTP-PCF, Station 15, EPFL
1015 Lausanne, Switzerland
Tel: +41 (0)21 693 06 51
E-mail: adrien.schmid@epfl.ch

**Keywords:** Alzheimer's disease; amyloid-beta, oligomers, antibody, immuno-therapy, aducanumab, LTP, synaptic plasticity, diagnostic.

**Author contributions:** AWS conceived the project, designed and directed the study. CEH and BG planned and carried out LTP studies. AWS performed mass spectrometry and biochemical analysis. JR and TS planned and carried out IF and array tomography studies on human brain tissue. GM and JSD carried out IF studies on Tg mouse brain. DD performed electron microscopy. VS carried out *C. elegans* experiments and analysis. MPF performed histological examination of human brain tissue. NR and AWS carried out ELISA measurements. BTH and MPF provided biological samples. AWS and CEH wrote the paper and all authors read and commented on the manuscript.

**Acknowledgments:** This work was funded by the "Enable Grant", kindly awarded by Dr. André Catana from the Technology Transfer Office (TTO) as well as the Catalyze4Life Innovation grant by Prof. Bart Deplancke and Dr. Kostas Kaloulis of the Ecole Polytechnique Fédérale de Lausanne (EPFL). We thank Dr. Adam Swetloff (TTO) for the constructive and strategic discussions on the project development as well as the support by the whole Life Sciences Faculty. The project was partially funded using internal funding of the EPFL. Human brain sample preparation and ELISA development was supported by the ADRC grant P30AG062421.We are grateful to the Roland Bailly Foundation (Geneva, Switzerland) for the funding of the MS instrument. We extend our gratitude to Dr. David Hacker (Protein Production and Structure Core Facility (EPFL) for his help with antibody production. Prof. Carmen Sandi, Laboratory of Behavioural Genetics (EPFL) for kindly providing us with antibodies for the study as well as Dr. Jose Sanchez-Mut, Laboratory of Neuroepigenetics (EPFL, Prof. J. Gräff lab), providing us with the reversed sequence of Aβ42-1 peptide and Prof. Hilal Lashuel (EPFL) for the Aβ40-arc mutant peptide. We thank Dr. Pamela Valdés (LEN, EPFL) for her support with IF imaging. TSJ and JR are funded by the UK Dementia Research Institute which receives its funding from DRI Ltd, funded by the UK Medical Research Council, Alzheimer's Society, and Alzheimer's Research UK, and the confocal used for IHC/AT was funded by Alzheimer's Research UK (ARUK-EG2016A-6) and a Wellcome Trust Institute Strategic Support Gant.

**Conflict of interest:** EPFL holds a patent on specific amyloid-beta peptide fragment signatures and the use thereof (WO2015150322).

**Abstract:**

In Alzheimer's disease (AD), Amyloid-beta (Aβ) oligomers are considered an appealing therapeutic- and diagnostic target. However, to date, the molecular mechanisms associated with the pathological accumulation or structure of Aβ oligomers remains an enigma to the scientific community. Here we demonstrate the strong seeding properties of unique Aβ fragment signatures and show that the truncated Aβ peptides of residues Aβ1-23, Aβ1-24 and Aβ1-25, rapidly seed to form small, SDS-PAGE stable assemblies of ~5kDa to ~14kDa molecular mass range. Mass spectrometry analysis of SDS-PAGE fractionated and gel extracted oligomers revealed that the truncated Aβ isoforms of residues 1-23 to 1-25 form stable entities with low molecular weight (LMW) oligomers, which strongly resemble the regularly reported Aβ entities of putative dimeric or trimeric assemblies found in human post-mortem AD and Tg mouse brain extracts. Furthermore, electrophysiological recordings in the mouse hippocampus indicate that LMW Aβ assemblies formed by fragments Aβ1-23 to Aβ1-25 significantly impair long-term-potentiation (LTP) in the absence of full-length Aβ1-42. Extensive antibody screening highlights the important observation, that the LMW Aβ assemblies formed by these truncated Aβ peptides escape immuno-detection using conventional, conformation specific antibodies but, more importantly, the clinical antibody aducanumab. Our novel findings suggest that there are new Aβ target "loopholes" which can be exploited for the development of therapeutic antibodies with binding properties against stable target hotspots present in Aβ oligomers. We provide here a first example of a new class of monoclonal antibody with unique binding properties against LMW Aβ oligomers, in the absence of binding to large fibrillar Aβ assemblies, or dense amyloid plaques. Our research supports a novel, unparalleled approach for targeting early, pathological Aβ species during the insidious phase of AD and prior to the appearance of large oligomeric or protofibrilar assemblies.

**Introduction:**

There is mounting evidence suggesting, that early therapeutic intervention will be the most promising therapeutic strategy in Alzheimer's disease (AD) (1). As a consequence significant effort has been made in the past to gain insight into early, "molecular triggers" associated with pathological amyloid-beta (Aβ) aggregation, because Aβ oligomers are known to play a causative role in early synaptic dysfunction and cognitive decline in patients suffering from dementia (2). Therefore, Aβ oligomers are widely accepted as an appealing diagnostic and therapeutic target (3) in Alzheimer's disease (AD). However, structural characterization of Aβ oligomers remains a challenging endeavour (4), which is mainly due to the labile and polymorphic nature found with these oligomeric entities. Consequently, it may not seem to be surprising, that the lack in clinical efficacy reported with earlier developed immuno-therapies collectively reflect the intrinsic difficulties observed with the characterization of a "unique pathological target" associated with neurotoxic Aβ oligomers.

The aetiology and neurotoxic properties of different, low molecular weight (LMW) oligomeric Aβ species (4–9) such as Aβ dimers and trimers (10) or, larger oligomeric assemblies (11), have been subjected to thorough studies in the past, in order to identify the "holy grail" of Aβ assemblies as novel therapeutic targets in AD (12). Numerous studies have narrowed down the search of pathological Aβ species to LMW species, namely dimers (10,13,14) or trimers (11). More recently, McDonald and colleagues (15) reported that human AD brain extracts contain small Aβ structures of a 6–7 kDa molecular mass range, of which these Aβ species may form part of larger, neurotoxic Aβ assemblies. However, earlier attempts to identify specific Aβ isoforms associated with LWM Aβ assemblies and, more specifically, the ~4kDa and ~7kDa species, have failed (16).

Aβ peptide mediated neurotoxicity has been the subject of a host of *in vitro* and *in vivo* electrophysiological studies, indicating that acute exposure of both, Aβ42 (17) and the more soluble Aβ40 (18,19) or, Aβ dimers isolated from human AD brains and CSF (14), significantly impair long-term-potentiation (LTP) in the rodent hippocampus. Earlier studies showed that intra-cerebral injection of Aβ40 in mice resulted in a rapid generation of truncated Aβ species (20), which resemble Aβ fragment fingerprints typically observed during *in vitro* Aβ oligomerization studies (12). The significance of truncated Aβ species is further supported by

Mazzitelli and colleagues (21), who reported that the co-occurrence of the truncated fragment Aβ1-24 promotes Aβ42 aggregation and impairs Aβ peptide clearance in the mouse brain. In strong support with this concept, we provided strong analytical evidence on an aggregation induced auto-cleavage and hence accumulation of a specific Aβ fragment fingerprint, which can rapidly seed to form oligomeric Aβ assemblies (12). Taken together, these findings suggest that a gradual accumulation of different truncated Aβ isoforms, of which some bear C-terminal amidation (-$CONH_2$), could play a central role in the early seeding events of Aβ oligomerization. These truncated Aβ species may therefore represent novel diagnostic markers as well as provide unprecedented therapeutic potential for the development of new antibody based AD therapies.

Using advanced technologies in quantitative and targeted mass spectrometry, together with our earlier developed neo-epitope antibody tools (12) against specific C-terminal truncated Aβ species, we were able to shed light on an enigma associated with LMW Aβ oligomers. Here we provide analytical proof of detection of specific truncated Aβ species present in LMW Aβ oligomers. This finding allows unprecedented and selective targeting of oligomeric assemblies, irrespective of oligomer structure or size. This gain in knowledge has led us to develop a novel, conformation selective mouse monoclonal antibody with unique binding properties against small oligomeric Aβ entities formed by the truncated Aβ isoforms Aβ1-23, Aβ1-24 and Aβ1-25, which appear during the early phase of Aβ peptide aggregation (12). In line with our antibody target design rational for early, LMW Aβ assemblies, we show that this novel antibody tool displays unique binding properties against LMW Aβ species, in the absence of binding to full-length Aβ42 monomers or higher order Aβ assemblies, such as amyloid plaques. We highlight here the strong need for identifying additional, molecular mechanisms associated with the early events of Aβ peptide aggregation during the long, insidious phase of AD. This in turn will allow the improvement of antibody-specific target engagement of early, pathological Aβ species present in the human AD brain and biofluids.

170
171
172
173 ***Results:***
174
175 ***Low molecular weight oligomers consist of an assembly of different C-terminally truncated***
176 ***Aβ isoforms.***
177 Numerous earlier reports show that oligomerization promotes the formation of labile Aβ
178 assemblies that decompose into SDS-PAGE stable Aβ entities of dimeric, trimeric and
179 tetrameric nature (12,15). Here, we have used a combination of analytical tools to investigate
180 the structural composition of these typical LMW Aβ assemblies observed during SDS-PAGE
181 analysis. Preparation of Aβ42 oligomers was carried out following a standardized and widely
182 applied protocol for the generation of amyloid derived diffusible ligands (ADDL) (22). In an
183 initial approach, Aβ oligomers were analysed by SDS-PAGE followed by immuno-blotting,
184 using the conventional antibodies 4G8 and 6E10, together with a selection of our earlier
185 developed, highly selective neo-epitope antibody tools (Table I & Supplementary Data Fig.
186 1a&b.) against different C-terminally truncated Aβ species (12).
187
188

| No. | Antibody | Target / Epitope | Host | Type | Applications tested | Source |
|---|---|---|---|---|---|---|
| **1** | N3 | Aβ C-term Asp23 | rabbit | polyclonal | IP, WB, DB | EPFL |
| **2** | N4 | Aβ C-term Val24-NH2 | rabbit | poylclonal | IP, WB, DB | EPFL |
| **3** | N5s | Aβ C-term Gly25-OH | rabbit | polyclonal | IP, WB, DB | EPFL |
| **4** | N5NH | Aβ C-term Gly25-NH2 | rabbit | polyclonal | IP, WB, DB | EPFL |
| **5** | N5ns | Aβ C-term 23-25 | rabbit | polyclonal | IP, WB, DB, ELISA, IHC | EPFL |
| **6** | JD1 | Aβ oligomer | mouse | monoclonal IgG1 | IP, DB, ELISA | EPFL |
| **7** | JD1 | Aβ oligomer | mouse | monoclonal IgM | DB, ELISA | EPFL |
| **8** | 6E10 | Aβ 3-8 | mouse | monoclonal | IP, WB, DB, ELISA, IHC | Covance |
| **9** | 4G8 | Aβ 17-24 | mouse | monoclonal | IP, WB, DB | Covance |
| **10** | MM26-2 | Aβ C-term 42 | mouse | monoclonal | WB | Anaspec |
| **11** | A11 | oligomers | rabbit | polyclonal | DB | Thermo-Fisher |
| **12** | OC | Aβ aggregates | rabbit | polyclonal | DB, IHC | Merck |
| **13** | Aducanumab | Aβ oligomers / fibrils | recombinant | human IgG | DB | Creative Biolabs |
| **14** | Neurogranin | - | sheep | polyclonal | WB | R&D Systems |
| **15** | Somatostatin | - | rabbit | polyclonal | WB | Abbexa |
| **16** | Syn-1 | alpha-synuclein | mouse | monoclonal | WB | BD Tansduction Labs |
| **17** | PSD94 | - | mouse | monoclonal | WB | abcam |
| **18** | b-actin | C-term | mouse | monoclonal | WB | Santa Cruz Biotech. |
| **19** | homer 1 | - | rabbit | polyclonal | WB | Synaptic Systems |

189
190 **Table I. Summary of the different antibodies used in the study.** Antibodies no. 1 to5 are referred to neo-epitope specific antibodies in the
191 study. IgM and IgG classes of the monoclonal antibody JD1 are shown, whereas the latter was mainly used in the study.
192
193
194

In line with earlier studies we show that, under denaturing SDS-PAGE conditions, large oligomeric assemblies dissociate into LMW species of putative dimeric, trimeric and tetrameric Aβ species (Fig. 1a). Probing the WB membrane with a combination of neo-epitope antibodies N-3, N-4 and N-5ns against Aβ fragments of residues 1-23 (mw: 2775Da), 1-24 (mw: 2875Da) and 1-25 (mw: 2932Da) respectively, allowed identification of C-terminally truncated Aβ species at the migration level corresponding to Aβ42 monomers, dimers, trimers and tetramers. Detection of these truncated Aβ fragments appeared to be significantly increased in Aβ42 tetramers when compared to trimers and dimers, whereas strong antibody signals were also observed at the Aβ42 monomer level (mw: 4512Da).

To confirm the identification of different Aβ species in LMW oligomers, we excised SDS-PAGE gel bands at the migration level of Aβ42 monomers to tetramers (Fig. 1b, inset: gel), followed by a repeated gel dehydration & rehydration process to allow diffusion of the gel trapped Aβ species into the solution. Following gel extraction, the solution containing different Aβ species was cleared and concentrated using C18 stage tips and subjected to MALDI-TOF/TOF MS analysis. MS analysis revealed a high abundance of fragments Aβ1-23 and Aβ1-25 together with full-length Aβ42 in the tetramer gel band (Fig. 1b; top spectrum). Similarly, the C-terminally amidated ($-NH_2$) forms of fragments Aβ1-24 and Aβ1-25 were also identified, however at significantly lower abundance. Overall, the MS signal intensities found for Aβ1-23 and Aβ1-25 were in line with the immuno-blot signal observed at the identical gel migration level of Aβ42 tetramers (≤15kDa) (Fig. 1a, lanes: 5&8). We could also identify similar Aβ fragment signatures in the trimer gel band, however, at significantly lower ratios when compared to tetramers, which corresponds to the decreased immuno-blotting signals found at the corresponding migration level.

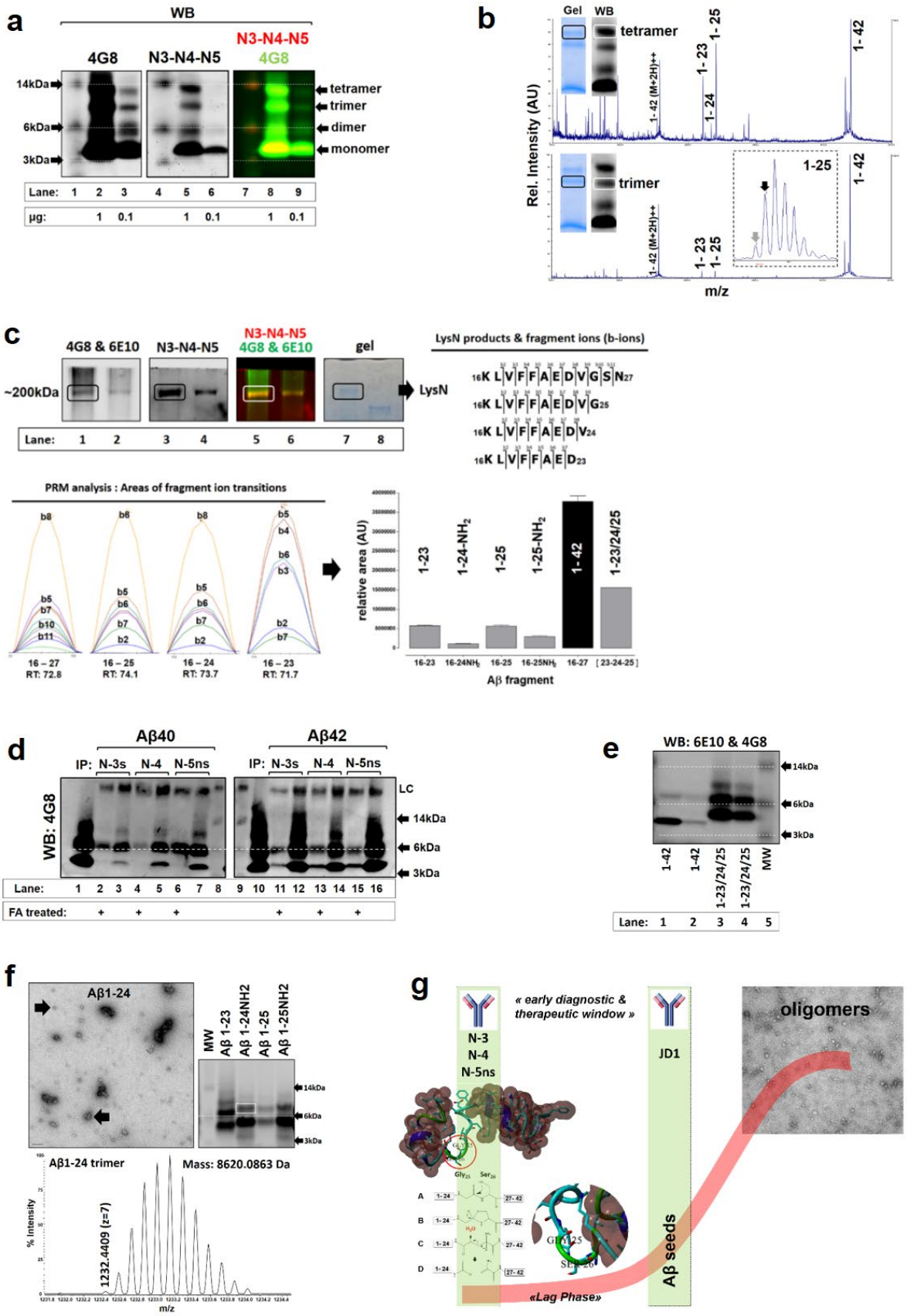
a
WB
4G8
N3-N4-N5
N3-N4-N5
4G8
14kDa
6kDa
3kDa
tetramer
trimer
dimer
monomer
Lane: 1 2 3 4 5 6 7 8 9
µg: 1 0.1 1 0.1 1 0.1
b
Gel
WB
tetramer
trimer
Rel. Intensity (AU)
1-42 (M+2H)++
1-23
1-24
1-25
1-42
m/z
c
4G8 & 6E10
N3-N4-N5
N3-N4-N5
4G8 & 6E10
gel
~200kDa
LysN
Lane: 1 2 3 4 5 6 7 8
LysN products & fragment ions (b-ions)
16K LVFFAEDVGSN27
16K LVFFAEDVG25
16K LVFFAEDV24
16K LVFFAED23
PRM analysis : Areas of fragment ion transitions
16 – 27 RT: 72.8
16 – 25 RT: 74.1
16 – 24 RT: 73.7
16 – 23 RT: 71.7
relative area (AU)
1-23
1-24-NH2
1-25
1-25-NH2
1-42
1-23/24/25
16-23
16-24NH2
16-25
16-25NH2
16-27
[23-24-25]
Aβ fragment
d
Aβ40
Aβ42
IP: N-3s N-4 N-5ns
IP: N-3s N-4 N-5ns
WB: 4G8
LC
14kDa
6kDa
3kDa
Lane: 1 2 3 4 5 6 7 8 9 10 11 12 13 14 15 16
FA treated: + + + + + +
e
WB: 6E10 & 4G8
14kDa
6kDa
3kDa
1-42
1-42
1-23/24/25
1-23/24/25
MW
Lane: 1 2 3 4 5
f
Aβ1-24
MW
Aβ 1-23
Aβ 1-24NH2
Aβ 1-25
Aβ 1-25NH2
14kDa
6kDa
3kDa
Aβ1-24 trimer
Mass: 8620.0863 Da
% Intensity
1232.4409 (z=7)
m/z
g
« early diagnostic & therapeutic window »
N-3
N-4
N-5ns
JD1
oligomers
Aβ seeds
«Lag Phase»

**Figure 1. Truncated Aβ species rapidly seed to form small oligomeric entities of 6-14kDa molecular weight range. a** left; SDS-PAGE and immuno-blotting (4G8) analysis of Aβ42 ADDLs, showing the typical gel migration pattern of Aβ dimers, trimers and tetramers within the molecular mass range of 6-15kDa. Samples were loaded at high (1ug) and low (100ng) concentrations. Centre IB; re-probed membrane with a mix of neo-epitope antibodies (N3, N4 & N5ns) revealing the presence of C-terminal truncated fragments. (IB right: merged scan of both antibodies at different wavelengths: green=800nm (4G8), yellow=680nm (N3, N4 & N5ns). Neo-epitope antibodies bind to specific bands at the migration level of putative Aβ42 tetramers, trimers and dimers. Substantial neo-epitope antibody binding was also observed at the Aβ42 monomer level, which indicates the presence of C-terminally truncated Aβ species present in this band. **b** MALDI-TOF/TOF analysis of gel extracted (by diffusion) Aβ species found in tetramers (top) and trimers (bottom). Aβ1-25 was partially detected as a C-terminal amidated form (inset grey arrow), whereas Aβ1-24 was predominantly detected as the C-terminal amidated form (Aβ1-24-$NH_2$). The strong MS signal intensities detected for Aβ23 and Aβ25, as compared to Aβ42 are in line with the IB signals found at the migration level of <14kDa (a). **c** WB and quantitative MS analysis of high molecular weight (HMW, ~200kDa) Aβ assemblies detected in the insoluble fraction. WB's were probed using either a combination of 6E10&4G (1$^{st}$ blot, left) followed by re-probing with a mixture of neo-epitope antibodies (2$^{nd}$ blot from left: N3, N4, N5ns & N5$NH_2$) to detect the presence of fragments Aβ 1-23 to 1-25 in these HMW oligomers. Gel bands were excised at the migration level of HMW oligomers and were subjected to LysN digestion, giving rise to the mid region sequences (inset right) of either 16-27 (from full-length Aβ1-42 cleavage) or 16-25 (e.g. derived from Aβ1-25 cleavage product). LysN cleavage products were subjected to PRM analysis and the calculated total peptide areas, as a sum of all $MS_2$ b-ion (b2 to b8) transitions (bottom, left), were used to estimate the relative abundance (histogram, right) of the different Aβ isoforms found within HMW oligomers. (Lanes 1-8 are identical Aβ samples but loaded at high (1, 3, 5) and low (2, 4, 6) concentrations, lane 8 = MWM). **d** WB analysis of Aβ40 (left) and Aβ42 (right) ADDLs. ADDLs were individually IP'ed with neo-epitope antibodies against fragments Aβ23, Aβ24 and Aβ25. Formic acid induced dissociation of ADDLs allowed a specific pull-down of these Aβ fragments (lanes: 2,4,6 and 11,13,15), whereas IP of native Aβ40 (lanes: 3,5,7) and Aβ42 (lanes: 12,14,16) ADDLs resulted in a pull-down of an oligomeric complex with substantial enrichment of a band centred at the migration level of ≥6kDa, which corresponds to a trimeric form of these Aβ fragments as seen by the migration pattern of a mixture of *in vitro* aggregated Aβ23 to Aβ25 (Figure 1e). (lanes: 1 & 10 = native Aβ40 & 42 ADDLs before IP, lanes: 8/9 = MW). **d** TEM imaging of the seeding properties observed with Aβ1-24, showing predominant spherical, oligomeric structures of 20-50nm diameter (arrows) and some clusters of larger aggregates (scale bar = 100nm). below; LC-MS analysis of Aβ24 trimers (WB inset) as seen by the multiply (m/z=1232.4409 $M+H^7$) charged ion. Inset right; WB analysis of the gel migration behaviour of individually aggregated fragments of Aβ23, Aβ24 and Aβ25. All Aβ fragments form substantial amounts of trimers centred at the migration level of >6kDa (white box: Aβ24) as confirmed by LC-MS analysis. A shift in migration profile can be observed between dimeric and trimeric Aβ23 and Aβ24 assemblies, which accounts for the difference in molecular mass (200-300Da) found for the Aβ24 species (see table 2 for comparison). **e** WB analysis of Aβ assemblies formed by the mixture of fragments Aβ1-23, 1-24 and 1-25. The rapid seeding of these fragments results in the formation of a substantial population of dimers (≥5kDa) and trimers (≥6kDa), with some tetramers (≤12kDa). Monomers (≤3kDa) are no longer observed and the dimer (≥5kDa) band is slightly shifted when compared to the Aβ42 monomers at 4.5kDa, which accounts for the difference in molecular mass for the dimeric species. (lanes: 1/2 = Aβ42 and lanes: 3/4 = Aβ23, 24 & 25 mixture at high and low concentrations). **f** Summary of neo-epitope antibody properties and application (left green bar) for targeted analysis of early fragment fingerprints as a result of Aβ aggregation. The design and development rational for a new conformational specific antibody (JD1) (right green column) with binding specificity against LMW oligomers (early seeds) derived from early Aβ fragment fingerprints of Aβ1-23 to Aβ1-25 is shown.

In addition to the above outlined diffusion extraction procedure, an identical copy of the gel bands was subjected to in-gel digestion, using LysN protease followed by LC-MS analysis, to further corroborate the findings by WB and MALDI-TOF MS, as well as to allow identification of additional Aβ isoforms present within these SDS-PAGE-stable LMW oligomers. High-resolution LC-MS analysis revealed the presence of a diversity of N-terminally, as well as C-terminally modified Aβ species across the different gel migration levels (Supplementary Data Fig. 1c-e). Generally, identification of fragments Aβ1-23, Aβ1-24 and Aβ1-25 could be confirmed in the monomer, dimer, trimer and tetramer bands and these fragments were found

271 to be significantly enriched in the monomer and tetramer bands respectively, which is in line
272 with the WB and MS analysis shown above (Fig. 1a). The increased abundance of truncated Aβ
273 species detected at the migration level of 3-5kDa may result from a gel migration induced
274 dissociation of Aβ assemblies, giving rise to the monomeric and dimeric form of Aβ1-23, Aβ1-
275 24 and Aβ1-25 (Table II). Moreover, LC-MS analysis allowed for unbiased identification of
276 the C-terminally amidated fragment Aβ1-24 ($Val_{24}$). In addition to the above listed truncated
277 forms, we were also able to identify C-terminal amidation at positions $His_{13}$, $His_{14}$ and $Asp_{23}$.
278 Modifications associated with the far C-terminal consisted of a repertoire of specific truncations
279 found at position $Gly_{37}$, $Gly_{38}$, $Val_{39}$ as well as $Ile_{41}$ (Supplementary Data Fig. 1e).
280
281
282

| Aβ Peptide | C-term. | Abbreviation | monoisotopic mass (Da) | average mass (Da) | Dimer (Da) | Trimer (Da) | Tetramer (Da) |
|---|---|---|---|---|---|---|---|
| 1-23 | COOH | 23 | 2775,27 | 2776,96 | 5554 | 8331 | 11108 |
| 1-24-NH2 | CONH2 | 24N | 2873,35 | 2875,11 | 5750 | 8625 | 11500 |
| 1-25 | COOH | 25 | 2931,36 | 2933,15 | 5866 | 8799 | 11733 |
| 1-25-NH2 | CONH2 | 25N | 2930,37 | 2932,16 | 5864 | 8796 | 11729 |
| 1-40 | COOH | 40 | 4327,15 | 4329,86 | 8660 | 12990 | 17319 |
| 1-42 | COOH | 42 | 4511,27 | 4514,10 | 9028 | 13542 | 18056 |

283
284 **Table II. List of Aβ peptide fragments used in the study.** Theoretical masses of Aβ dimers, trimers and tetramers was calculated using the
285 average peptide mass.
286
287
288

289 **Truncated Aβ species may seed to form SDS-PAGE stable entities with large Aβ**
290 **oligomeric assemblies of a 50-200kDa molecular mass range.**

291 We reasoned that the detection of small Aβ assemblies at the migration level of 5-14kDa may
292 result from the dissociation of larger (≥30kDa), metastable Aβ entities. We therefore decided
293 to analyse the insoluble fraction after centrifugation of the ADDLs (soluble fraction)
294 preparation. This insoluble fraction is known to contain mainly large Aβ assemblies of
295 protofibrillar and fibrillar nature (data not shown). WB analysis of this fraction revealed the
296 presence of different, large Aβ assemblies at the migration level of 50kDa to 200kDa
297 (Supplementary Data Fig. 2a). Probing the membrane with antibodies directed against the N-
298 terminal (6E10) and mid-region (4G8) or, the C-terminal ending of Aβ42 (MM26-2) (Table I)
299 allowed the identification of the bulk of Aβ assemblies centred at the LMW migration level of
300 4-14kDa, as observed with the soluble ADDL fraction shown above. However, application of
301 a cocktail of neo-epitope antibodies (N3, N4, N5ns and N5NH2) also strongly indicated the

presence of distinct Aβ assemblies found at the gel migration level of ~200kDa (Fig. 1c) as well as ~98kD, ≥62kDa and ≥50kDa (Supplementary Data Fig. 2a). We observed particularly strong binding of 6E10 & 4G8 as well as N3-N5 (mix) to a large Aβ entity found at ~200kDa (Fig. 1c, top: WB). We therefore decided to carry out in-gel digestion followed by quantitative MS analysis of these large Aβ entities in order to confirm the presence of the different Aβ isoforms of Aβ1-23 to Aβ1-25 within these stable assemblies. Our quantitative MS analysis confirmed the high abundance of the different Aβ isoforms of 1-23, 1-24$NH_2$, 1-25 and 1-25$NH_2$ present in these large Aβ assemblies (e.g. 200kDa) of which the overall calculated sum of all truncated Aβ isoforms accounted ≥40%, when compared to full-length Aβ1-42 (Fig. 1c, bottom: histogram). We also provide quantitative MS data on the different Aβ isoforms detected at the gel migration level of ≥50kDa, ~98kDa and ~200kDa (Supplementary Data Fig. 2b).

**Dissociation of Aβ oligomers results in the isolation of Aβ species of 6kDa to 14kDa mass range.**

Given the observation that truncated Aβ species form stable complexes with LMW and HMW oligomers, we were interested in validating if we are able to pull-down Aβ oligomers formed by Aβ40 or Aβ42 peptides. To address this question, we prepared ADDLs of which one part of the preparation was subjected to 70% formic acid (FA) denaturing (3hrs at room temp.) followed by IP using neo-epitope antibodies N-3s, N-4 or N-5ns (Table I & Supplementary Data Fig. 1a&b). We show that selective IP of FA dissociated ADDLs resulted in a specific capturing of two Aβ species centred at the gel migration level of 6kDa and <14kDa, whereas IP of native (not denatured) ADDLs resulted in the pull-down of the typical oligomeric assemblies found at a migration level of 6-14kDa (Fig. 1d). The selective pull-down and therefore isolation of the ≥6kDa Aβ species was found to be more straightforward with Aβ40 assemblies (Fig. 1d, left; lanes 2-7), whereas Aβ42 ADDLs appeared to be more resistant to FA dissociation (Fig. 1d, right; lanes: 11-16).

336 **Aβ fragments of Aβ1-23, Aβ1-24 and Aβ1-25 rapidly seed to form SDS-stable, LMW**
337 **assemblies in the absence of full-length Aβ1-42.**
338 Because our earlier studies strongly indicated that Aβ aggregation is accompanied by the
339 appearance of the typical fragment fingerprint consisting of truncations at residues 1-23, 1-24
340 and 1-25, we were interested in understanding the seeding properties using a mixture of these
341 C-terminally truncated Aβ species. We show that, *in vitro* aggregation of these truncated Aβ
342 fragments results in the rapid formation of stable assemblies within the 5-15kDa molecular
343 range, of which dimers (≥5kDa) and trimers (≥6kDa) are the most predominant species formed
344 by these Aβ fragments, whereas monomers (theoretical av. mass range: 2776Da to 2933kDa)
345 were no longer detected (Fig. 1e, lanes: 3-4). Consistent with this observation, earlier reports
346 showed a rapid seeding behaviour with fragment Aβ1-28, revealing gel migration profiles that
347 are consistent with stable Aβ1-28 dimers (22). The gel migration profile of the peptide mixture
348 of Aβ1-23 to Aβ1-25 dimers (>5kDa) was significantly shifted when compared to full-length
349 Aβ1-42 monomers (4.5kDa) (Fig. 1e, lanes 1-2), whereas the trimeric form of these truncated
350 Aβ species (theoretical mass: 8-9kDa) was found at a migration level above ≥6kDa, which
351 strongly resembles the migration profile of earlier reported putative Aβ42 dimers (10) or 4-
352 7kDa assemblies (15) isolated from human AD brain extracts.
353 We then investigated the self-seeding properties of individual truncated Aβ species Aβ1-23,
354 Aβ1-24-$NH_2$ and Aβ1-25 as well as the C-term amidated form of Aβ1-25 ($NH_2$). In vitro
355 aggregation of Aβ1-24 showed that this fragment has rapid self-seeding properties, resulting in
356 the formation of SDS-PAGE stable assemblies in the MW range of dimers to trimers (Fig. 1f,
357 WB inset). Transmission electron-microscopy (TEM) imaging revealed that fragment Aβ1-24
358 preferentially seeds to form homogenous spherical aggregates with some clusters of small
359 protofibrillar structures. The gel migration profile of Aβ1-24 and Aβ1-25 peptides were similar
360 (Fig. 1f), whereas the gel migration profile appeared to be slightly shifted when compared to
361 fragment Aβ1-23, which may account for the difference in MW between these Aβ species
362 (Aβ23 vs. Aβ24 dimer = 198Da, Aβ24 dimer vs. Aβ25 dimer = 114Da) (Table II).
363 The true molecular entity of these small oligomeric assemblies observed by SDS-PAGE was
364 further confirmed using high-resolution LC-MS analysis, revealing the presence of highly
365 stable Aβ1-24 trimers (8.6kDa) (Fig. 1f, bottom: MS spectrum) as well as dimers (5.7kDa) or
366 even pentamers (14.3kDa) (Supplementary Data Fig. 2c-d). The MS analysis of stable dimers
367 to pentamers of these truncated Aβ peptides further corroborates the migration pattern observed
368 by denaturing SDS-PAGE analysis (Fig.1f, WB inset), and therefore rules out any analytical
369 artefacts associated with gel migration (23).

370 ***Detection of early, pathophysiological Aβ seeds requires the development of novel antibody***
371 ***tools, with high binding selectivity for small oligomeric assemblies, in the absence of***
372 ***monomer binding.***
373 The above reported findings clearly highlight the need for the development of additional
374 antibody molecules with high binding specificity for LMW Aβ oligomers, irrespective of the
375 presence of the full-length Aβ42 or Aβ40 target. To address this limitation, we set out to develop
376 a conformational specific antibody; with preferential binding properties against a repertoire of
377 LMW Aβ assemblies formed by here described truncated Aβ species. We speculated that the
378 application of such a conformation specific antibody would serve as an additional analytical
379 tool as compared to our earlier developed neo-epitope antibodies, therefore allowing the
380 detection of the gradual appearance of small Aβ entities, prior to the accumulation of large,
381 metastable oligomeric or protofibrillar species (Fig. 1g).
382 We therefore immunized mice using a synthetic, oligomeric form of fragment Aβ1-24 and
383 screened clones for antibodies with binding properties against a linear (denatured), and
384 aggregated (positive target) form of the different C-terminally truncated Aβ fragments of
385 interest as well as against denatured, full-length Aβ42 and Aβ40 peptide (negative target).
386 Using a combination of ELISA and DB techniques, we were able to identify six antibody-
387 secreting clones (data not provided), with different antibody binding properties against
388 oligomeric Aβ assemblies of interest, of which the properties of one selected monoclonal
389 antibody (mAB), referred to as **"*JD1*"** is described below.
390
391
392 **The monoclonal antibody JD1 binds LMW Aβ assemblies, which appear during the early**
393 **time course of Aβ aggregation.**
394 To characterize the binding specificity of JD1, we initially compared JD1 binding properties
395 with the two conventional antibodies 4G8 and 6E10, as well as different, conformation specific
396 antibodies such as the A11 or OC antibody. We found that the intrinsic binding property of
397 JD1 is not limited to fragment Aβ1-24, since JD1 binding was also observed for the different
398 aggregated forms of fragments of Aβ1-23 and Aβ1-25-$NH_2$ (Fig. 2a; bottom DB). Immuno-
399 blotting analysis indicated that JD1 positive signals found by dot blotting are in agreement with
400 the presence of LMW oligomeric assemblies found at the Aβ peptide migration range of dimers
401 and trimers (5-14kDa) and this could be also confirmed using aggregated Aβ42 (Fig. 2a, top
402 WB, lane: 6). While JD1 clearly binds to oligomeric Aβ assemblies using native DB, we do not
403 observe positive JD1 binding of these LMW species by WB. The reason for this observation

404 may result from either dissociation of larger (≥ 14kDa) Aβ assemblies or from a SDS-PAGE
405 induced denaturing of the conformational epitope.
406 DB analysis of Aβ aggregation kinetics indicated that significant JD1 binding can be observed
407 following ≥8hrs aggregation of the full-length, wild type (wt) Aβ1-42 peptide (Fig. 2b).
408 Remarkably, aggregation kinetics analysis of the arctic mutant Aβ40 revealed that, JD1 binding
409 significantly preceded the detection of oligomeric assemblies formed by Aβ40-Arc peptide,
410 when compared to wt Aβ42 peptide. TEM imaging indicated that selective JD1 binding was
411 accompanied by the presence of predominantly oligomeric entities found with Aβ40-Arc (Fig.
412 2b), which is in line with the morphology observed with fragment Aβ1-24 (Fig. 1f). Probing
413 Aβ42 peptide aggregation with neo-epitope antibodies revealed that the rise in JD1 positive
414 species is generally associated with a gradual accumulation of C-terminally truncated Aβ
415 species of residues 1-23 to 1-25 and this was further confirmed by MALDI-TOF MS (Fig. 2c,
416 bottom: MS spectrum), whereas no antibody binding was observed for the more soluble, wt
417 Aβ40 peptide during the same time course of peptide aggregation (Fig. 2c; top DB).
418
419

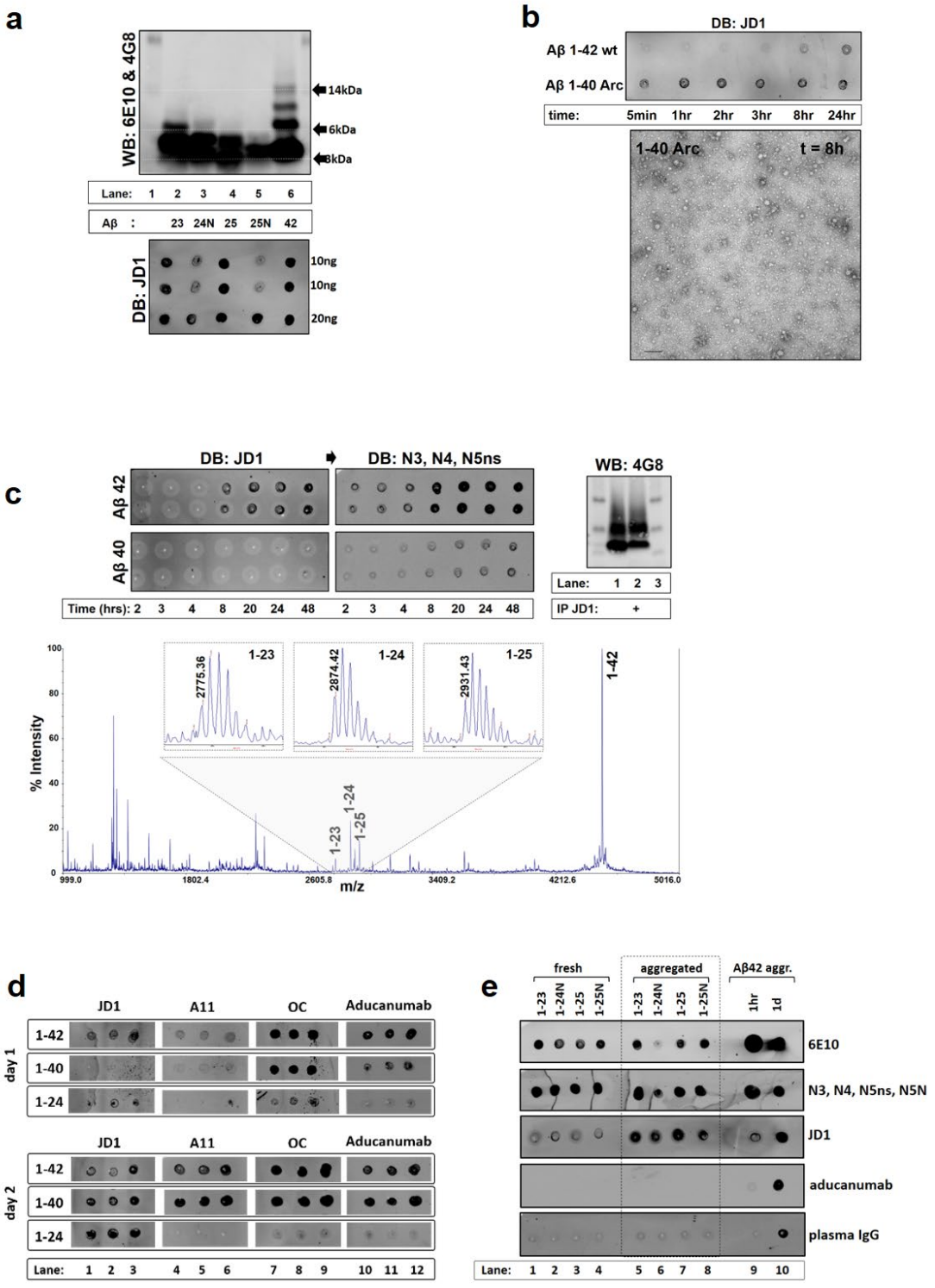
a
WB: 6E10 & 4G8
14kDa
6kDa
3kDa
Lane: 1 2 3 4 5 6
Aβ : 23 24N 25 25N 42
DB: JD1
10ng
10ng
20ng
b
DB: JD1
Aβ 1-42 wt
Aβ 1-40 Arc
time: 5min 1hr 2hr 3hr 8hr 24hr
1-40 Arc
t = 8h
c
DB: JD1
DB: N3, N4, N5ns
Aβ 42
Aβ 40
Time (hrs): 2 3 4 8 20 24 48 2 3 4 8 20 24 48
WB: 4G8
Lane: 1 2 3
IP JD1: +
% Intensity
m/z
1-23
1-24
1-25
1-42
2775.36
2874.42
2931.43
d
JD1
A11
OC
Aducanumab
day 1
day 2
1-42
1-40
1-24
Lane: 1 2 3 4 5 6 7 8 9 10 11 12
e
fresh
aggregated
Aβ42 aggr.
1-23
1-24N
1-25
1-25N
1hr
1d
6E10
N3, N4, N5ns, N5N
JD1
aducanumab
plasma IgG
Lane: 1 2 3 4 5 6 7 8 9 10

**Figure 2. LMW Aβ oligomers escape immuno-detection using conventional, conformation specific antibodies. a** WB (4G8 & 6E10) and DB (JD1) analysis of the migration profile of JD1 positive species formed by aggregated Aβ1-23 to Aβ1-25 (lanes: 2-4) and full-length Aβ42 (lane: 6). The presence of Aβ42 (lane 6) species at the migration level of dimers and trimers is revealed by WB analysis. Below; DB validation of JD1 positive species. JD1 positive signals found for Aβ42 were associated with the presence of bands detected at ≥6kDa and ≤14kDa (lane: 5). **b** Aggregation kinetic analysis of the mutant Aβ40-Arc versus wt Aβ42 peptide using JD1 (DB) and TEM imaging of Aβ40-Arc oligomers at 8hrs. Aβ entities of spherical (10-50nm) and small protofibrillar morphology can be observed with Aβ40-Arc (scale bar = 100nm). **c** Monitoring of Aβ42 and Aβ40 aggregation kinetics using JD1 and MS. top: DB validation using JD1 (left) and re-probed with a mixture neo-epitope antibodies (right): positive JD1 signals are observed following 8hrs of Aβ42 aggregation (DB) and this was accompanied by an appearance of fragments Aβ23, Aβ24 and Aβ25 as probed with N3, N4 and N5ns (right). Bottom: MS (MALDI-TOF-TOF) analysis of Aβ fragment signatures detected at t=8hrs. Inset right; WB analysis of IP'ed (JD1) Aβ42 (t=8hrs) (lane 2) showing the pull-down of a predominant band centred at the migration level of ≥6kDa. (lane 1: Aβ42 starting material). **d** DB validation of Aβ40 and Aβ42 as well as truncated Aβ1-24 aggregation kinetics using JD1 (Lanes: 1-3), the oligomer specific antibody A11 (lanes: 4-6), conformation specific antibody OC (lanes: 7-9) and Aducanumab (lanes: 10-12) (samples were spotted at two different concentrations: lanes 1-2, 4-5, 7-8,10-11 = 50ng and lane 3, 6, 9, 12 = 100ng). A clear difference in antibody binding to aggregated Aβ24 can be seen between JD1 and A11 as well as Aducanumab. **e** Validation of JD1, Aducanumab as well as human plasma, natural IgGs or 6E10 binding specificity against freshly prepared (lanes: 1-4) or aggregated (lanes: 5-8) forms of Aβ fragments Aβ23, Aβ24 and Aβ25 as well as Aβ42 (lanes: 9-10). JD1 has strong binding affinity for the aggregated form of the different Aβ fragments; whereas no binding was observed with Aducanumab or plasma IgGs (lanes. 5-8) against the soluble or aggregated form of these C-term truncated Aβ species.

## Validation of JD1 binding properties against oligomeric Aβ species and its potential applications for screening methods.

We show that detection of JD1 positive species was accompanied by the gradual accumulation of a typical Aβ fragment fingerprint (Aβ23 to Aβ25) as shown by the application of neo-epitope antibodies (Supplementary Data Fig. 3a) and JD1 proved to be useful for screening aggregation inhibitors, such as the green tea extract (EGCG) (Supplementary Data Fig. 3b). In line with the DB screening we show that, IP-MS analysis with JD1 does not result in the pull-down of soluble, Aβ42 monomers at early time points (t ≤ 30min), when compared to prolonged aggregation times (t = ≥2hrs) (Supplementary Data Fig. 3c). We also took advantage of the C. elegans GMC101 worm model to further understand the binding property of JD1 using a living organism. GMC101 worms constantly express the human Aβ42 isoform in muscle cells and develop age-progressive paralysis and significant amyloid deposition which are A11 positive species (24). WB analysis of aged GMC101 worms revealed a significant accumulation of different LMW Aβ species at the molecular weight range of 5-14kDa. IP-MS analysis of GMC101 extracts confirmed the abundance of different C-terminal truncated Aβ species (Supplementary Data Fig. 3d), which reflects the typical Aβ fragment signatures found in Tg2576 mice and human post-mortem brain tissue extracts (25). Furthermore, we show that JD1 also binds oligomeric assemblies formed by synthetic mouse Aβ42 sequence, though, with significantly lower affinity (Supplementary Data Fig. 3e), whereas, no binding was observed

468 against the reversed human Aβ42-1 sequence (Supplementary Data Fig. 3f) or aggregated
469 alpha-synuclein protein (data not shown). These observations collectively rule out JD1's
470 binding property against oligomeric assemblies formed by other amyloidogenic proteins, as
471 observed with earlier developed conformation specific antibodies (26). Collectively these
472 observations highlight JD1's unique binding property for predominantly, small oligomeric Aβ
473 assemblies, in the absence of binding of full-length Aβ1-42 or Aβ1-40 monomers.
474
475
476 **Small Aβ assemblies formed by the N-terminal fragments Aβ1-23 to Aβ1-25 are not**
477 **detected by conventional, anti-oligomeric antibodies or natural plasma IgG's.**
478 Due to the strong seeding properties observed with C-terminally truncated Aβ species, we
479 investigated if these LMW oligomeric assemblies can be detected using conventional, anti-
480 oligomeric antibody tools. For this purpose, full-length Aβ42 and Aβ40, as well as the C-
481 terminally amidated fragment Aβ1-24-NH2 were subjected to aggregation kinetics and probed
482 with the "anti-oligomer" specific antibody A11 and the "conformation-specific" antibody OC
483 (6,26,27), as well as a biosimilar of the clinical antibody aducanumab (28,29). No visible
484 antibody binding was observed at day 0 (data not shown), which is in line with earlier reported
485 antibody screening studies using A11 and OC (30). Following one day of Aβ peptide
486 aggregation, significant antibody binding was only observed against peptides Aβ42 and Aβ40
487 using the OC and aducanumab antibodies (Fig. 2d), whereas A11 reached a similar level of
488 binding significance following two days of aggregation. Generally, positive immuno-probing
489 signals for Aβ42 preceded the detection of Aβ40 oligomers, which is likely due to the increased
490 aggregation propensity found with Aβ42. At day two, JD1 binding to aggregated Aβ42 and
491 Aβ40 was similar when compared to aducanumab, but with a noticeable lag in detection of
492 Aβ40 at day 1. Intriguingly, our screening studies revealed a striking difference in antibody
493 binding affinity for the aggregated Aβ1-24 peptide. Detection of oligomeric Aβ1-24 assemblies
494 was significantly reduced using the OC or aducanumab antibody and absent with A11 (Fig. 2d
495 & Supplementary Data Fig. 3g). To determine if the intrinsic binding properties of JD1 are
496 associated with an oligomeric or linear, denatured form of Aβ peptide, we prepared fresh Aβ
497 peptide standards by dissolving and sonicating the Aβ peptides in HFIP solution, followed by
498 solution evaporation and solubilization in a 50mM NaOH solution as described earlier (30).
499 Sample preparation of freshly prepared (t=0) or aggregated (t=1d) Aβ peptide standards where
500 screened by DB using JD1 and aducanumab, together with a cocktail of neo-epitope antibodies
501 (N3, N4, N5ns, N5N) as well as 6E10 for the detection of all Aβ assemblies. Our findings

strongly indicate that JD1 has significantly increased binding properties for the aggregated form of fragments Aβ1-23, Aβ1-24-$NH_2$, Aβ1-25, Aβ1-25$NH_2$ and that detection of these Aβ species was significantly reduced with aducanumab (Fig. 2e, lanes: 5-8). Application of neo-epitope antibodies enabled the detection of both, denatured as well as aggregated forms of the Aβ peptide, indicating that these antibodies bear high C-terminal binding specificity, irrespective of Aβ peptide structure, which is in agreement with our earlier reported validation studies (12). Human plasma is known to contain natural IgGs antibodies that are reactive against a broad range of different amyloidogenic species. Because natural antibodies have been reported to bear neuroprotective properties against Aβ peptide (31–33), we were interested in understanding if these plasma IgG's also bear binding properties against the here described LMW Aβ oligomers. In-spite of the high, natural abundance of conformation-specific antibodies reported in human plasma, we could not identify plasma IgG selective binding to the small oligomeric Aβ entities of fragments Aβ1-23 to Aβ1-25. However, significant plasma IgG binding was observed for aggregated, but not soluble Aβ42 peptide and levels of plasma IgG binding was comparable with aducanumab (Fig. 2e, lane: 10). Overall, these observations highlight the important finding that, the small oligomeric Aβ assemblies formed by the truncated fragments Aβ1-23 to Aβ1-25, may escape conventional immuno-based detection, using the oligomer-specific antibody A11 or aducanumab.

***Identification of JD1 positive assemblies in human post-mortem AD brains highlights the pathological significance of LMW Aβ assemblies in AD.***

To further provide evidence of the significance of LMW oligomeric Aβ species in AD brains, we decided to screen biological samples using a combination of immuno-fluorescence (IF) and array tomography imaging as well as IP-MS and ELISA assays. Having confirmed the presence of truncated Aβ fingerprints in a set of human brain samples earlier (12), we set out in specifically identifying JD1 positive species in post-mortem human brains.

IF imaging of human AD brains revealed the presence of dense core plaques, which were thioflavin S (ThioS) and OC positive, however, we did not observe any JD1 positive staining of these dense amyloid plaques (Fig. 3a). Therefore, we were interested in identifying the presence of JD1 positive species at synapses, because one of the early and important effects of oligomeric Aβ in AD, is the binding of oligomeric Aβ to synapses, resulting in synaptic dysfunction and gradual loss of synapses. Tissue from human subjects was prepared for high-resolution ribbon array tomography as reported previously (34), allowing accurate and high-

resolution detection of individual synapses. Similar to our IF analysis, application of the OC antibody resulted in strong labelling of dense core Aβ plaques as well as individual postsynaptic punctae, which co-localized with PSD95 protein staining. No JD1 positive staining could be observed for dense Aβ plaques, which is in line with the IF analysis of aged (≥9months) Tg2576 mouse brains (data not shown). Interestingly, we clearly observed selective JD1staining at individual postsynaptic punctae, which co-localized with OC and PSD95 staining (Fig. 3b). This observation indicates that JD1 positive Aβ assemblies may represent early, neurotoxic Aβ species associated with synapse binding and therefore resulting in gradual neurodegeneration.

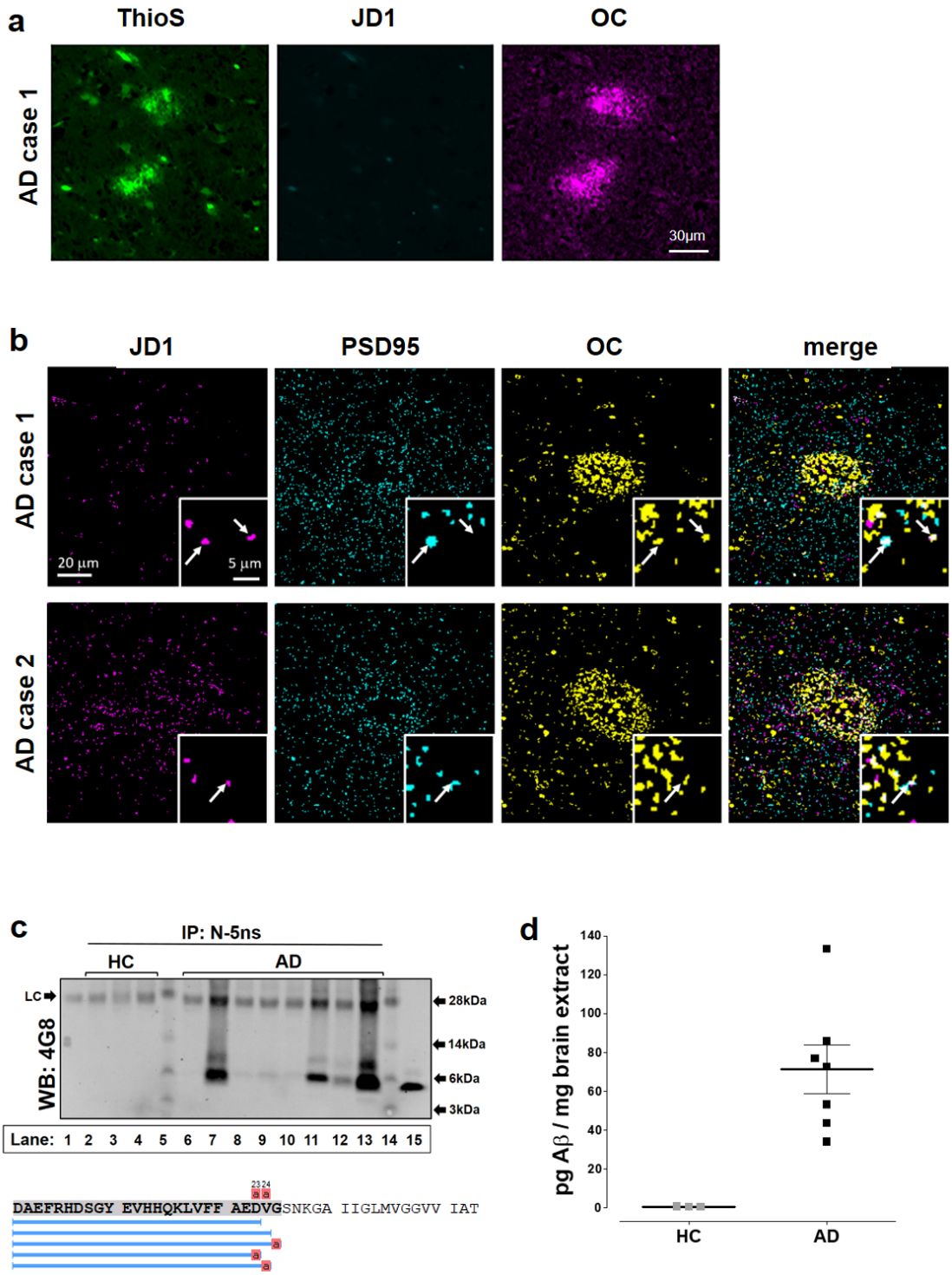
a
ThioS
JD1
OC
AD case 1
30µm
b
JD1
PSD95
OC
merge
AD case 1
20 µm
5 µm
AD case 2
c
IP: N-5ns
HC
AD
LC
WB: 4G8
28kDa
14kDa
6kDa
3kDa
Lane: 1 2 3 4 5 6 7 8 9 10 11 12 13 14 15
DAEFRHDSGY EVHHQKLVFF AEDVGSNKGA IIGLMVGGVV IAT
d
pg Aβ / mg brain extract
140
120
100
80
60
40
20
0
HC
AD

556 **Figure 3. JD1 positive oligomers are detected in the post-synaptic vicinity of AD brains. a** IF staining of amyloid plaques found in a
557 human AD brain, using Thioflavin S (Thio S), JD1 and OC antibody. Significant plaque staining was observed with Thio S, which co-localized
558 with OC staining, whereas no staining of dense core plaques was found using JD1. **b** Array tomography images of Aβ deposits detected in
559 two post-mortem human AD brains using JD1, anti-PSD95 and OC antibody (left to right). JD1 positive species were detected in the post-
560 synaptic vicinity, which co-localize with PSD95 positive staining. Large images are maximum intensity projections of 5 serial sections and
561 insets are single sections confirming colocalization**.** (for brain tissue details see Supple. Table I). **c** Example of an IP-WB analysis of human
562 cortical brain tissue extracts using the neo-epitope antibody N5ns. Significant pull-down of dimeric and trimeric Aβ species are observed in
563 a majority of AD (lanes 6-14) but not control (lanes 2-4) brains. (lane 1: IgG ctrl, lane 15: MW, Lane 16: aggregated synthetic Aβ25 dimer).
564 Below; Representative summary of an IP-MS analysis of an AD brain sample (lane 14) using a mixture of antibodies N3, N4 and N5ns. Blue
565 bars highlight the sequences of all Aβ species identified (FDR ≤1%) (PEAKS Studio soft.) **d** ELISA analysis of JD1 positive assemblies found
566 in post-mortem human AD (n=7) brains (FA extracts) but not in age matched controls (HC, n=3). (range: 35pg-132pg / mg brain tissue)
567 (median ± SEM of technical triplicates).
568
569

570 **Targeted mass spectrometry analysis of human AD brain extracts reveals the presence of**
571 **LMW Aβ assemblies, consistent with the detection of fragments Aβ1-23 to Aβ1-25.**

572 We decided to analyse human post-mortem brains to further support the results of our high-
573 resolution array-tomography and provide insight into the pathophysiological significance of
574 these truncated Aβ isoforms as well as the LMW oligomers. We employed IP-WB and IP-MS
575 analysis of eight AD and three human control (HC) brain extracts (Supplementary Data Table
576 I) and found that IP with N-5ns enabled the isolation of Aβ species centred at a gel migration
577 level of 5-6kDa and ≥6kDa, which corresponds to our above observed dimeric and trimeric
578 species of fragment Aβ1-25 (Fig. 1e). Significant levels of dimeric and trimeric Aβ species
579 were detected in four AD brains (Fig. 3c, lanes: 7, 12 13 & 14), whereas the detection of these
580 Aβ species was significantly lower in three other AD subjects (Fig. 3c, lanes: 8-10). No Aβ was
581 detected in brains from human controls (Fig. 3c, lanes: 2-4) as well as in one AD subject (lane:
582 6). Generally, IP-WB analysis of these AD brain extracts strongly resembled the migration
583 profile of the above reported FA dissociated ADDLs (Fig. 1d). Moreover, using IP-MS analysis
584 with a neo-epitope antibody cocktail (N3, N4, N5ns), we were able to confirm the overall
585 presence of different Aβ species in AD brain extracts but not human controls (Fig. 4c; bottom
586 inset & Supplementary Data Fig.4a-e). Overall, our IP-MS analysis allowed the unbiased
587 identification of different truncated Aβ species of residues 1-23, 1-24, 1-25, of which fragment
588 1-24 was predominantly detected as a C-terminal amidated (-$CONH_2$) form. In addition, we
589 were also able to identify the C-terminally amidated fragment of Aβ1-25 (Supplementary Data
590 Fig. 4e) using a recently developed neo-epitope antibody (N-5NH2) (Table I).
591 Next, we carried out protein extractions from Tg2576 mouse (age: 9months) brain tissue as well
592 as human post-mortem AD and HC brains, using either TBS, formic acid (FA) or SDS
593 extraction buffers, followed by immuno-precipitation with JD1 and downstream targeted MS

analysis. IP-MS analysis of Tg2576 mice and human AD brains provided unbiased confirmation of the presence of JD1 positive Aβ assemblies in these brain samples (Supplementary Data Fig. 5a) and detection of these Aβ species was found to be increased using FA and SDS extraction buffers, when compared to the more soluble TBS fractions, which is an observation also reported by others (10). However, we cannot rule out that the use of harsh extraction buffers, such as FA, could eventually result in substantial dissociation of small oligomeric Aβ assemblies, therefore contributing to a decrease or even loss of the conformational epitope associated with JD1 binding.

To further corroborate the presence of JD1 positive species in post-mortem human brain, we next, applied a sandwich ELISA (Supplementary Data Fig. 5b), using JD1 as capture antibody and a biotinylated form of 6E10 for detection of oligomeric Aβ species in HC (n=3) and AD (n=7) cortical brain tissue extracts. Our ELISA measurement revealed that, JD1 positive assemblies can be detected in all of the AD subjects, though, with considerable inter-subject variability (30-140pg / mg cortical brain extract), which may reflect the general variability in Aβ pathology found in AD subjects (Fig. 3d). Indeed, a large inter-subject variability of LMW Aβ assemblies was also observed by IP-WB (Fig. 3c). No JD1 positive species were detected in brain extracts from control subjects, however, the low number of subjects used here would not rule out the presence of low amounts of oligomeric Aβ in other, age matched control subjects or patients suffering from MCI (35).

Collectively, our brain imaging and screening studies strongly indicate that JD1 has preferential binding properties against small Aβ assemblies and that antibody binding may be gradually lost during the time course of on-pathway Aβ peptide aggregation. This may also explain the lack in JD1 binding to dense core plaques as well as the decrease in JD1 binding affinity following extended (≥2week) Aβ peptide aggregation (Supplementary Data Fig. 3b). Nevertheless, our findings do not rule out binding of JD1to protofibrillar or fibrillar structures, given that the Aβ binding epitope is sufficiently conserved and more importantly exposed, in these larger Aβ assemblies.

627 ***LMW oligomers formed by fragments Aβ1-23 to Aβ1-25 significantly impair synaptic***
628 ***plasticity.***
629 Earlier reports showed that unlike full-length Aβ42, the truncated form of Aβ1-16 did not have
630 any inhibitory effects on synaptic plasticity (36), whereas other reports indicate that the larger
631 Aβ1-25 isoform, serves a sphingolipid-binding domain motif and is rapidly internalized by
632 neuronal cells (37). This rapid peptide internalization may account for the acute neurotoxicity
633 observed for some Aβ fragments. Therefore, to address the acute neurotoxic properties of
634 truncated Aβ species, we decided to generate LMW oligomers using a mixture of the typically
635 observed Aβ fragment fingerprints during aggregation. For this purpose, a mixture of the
636 synthetic Aβ fragments Aβ1-23, Aβ1-24-NH2, Aβ1-25 and Aβ1-25-NH2 (50ng/ul) was
637 incubated over-night followed by size exclusion chromatography (SEC) purification of LMW
638 oligomeric assemblies that are recognized by JD1.
639 We identified JD1 positive Aβ species in the elution volume (13ml) corresponding to the mass
640 of a theoretical molecular standard of ≥13.7kDa (Fig. 4a). WB analysis of the SEC fractions
641 revealed a population of different Aβ assemblies of molecular weights ranging from ≥5kDa
642 (dimers) to ≥ 6kDa (trimers), though we cannot rule out that these Aβ entities are the result of
643 the SDS-PAGE analysis induced dissociation of larger Aβ assemblies. MS analysis of the JD1
644 positive fraction confirmed the identification of a mixture of all four Aβ isoforms present in the
645 JD1 positive fraction (data not shown).
646

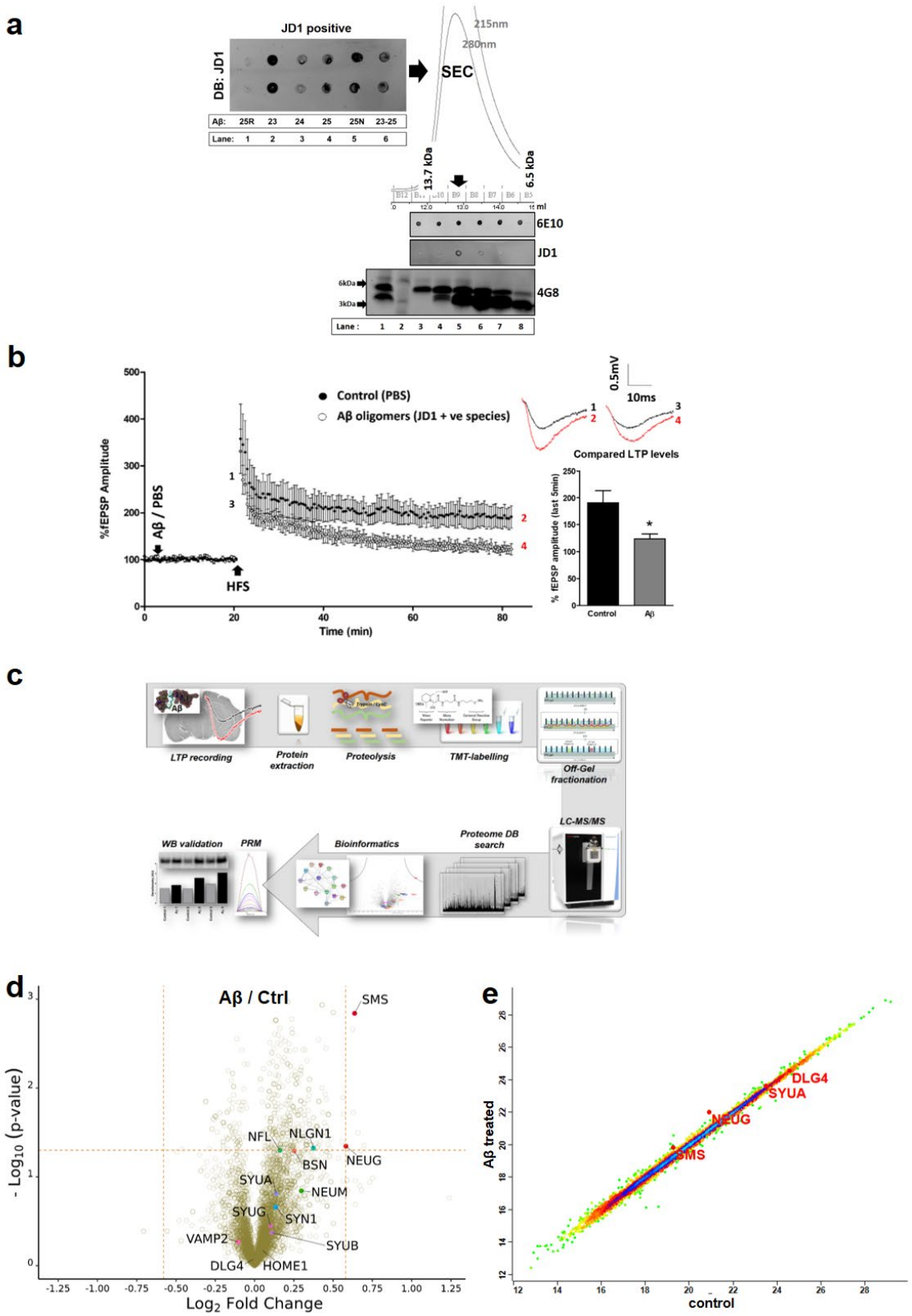
a
JD1 positive
DB: JD1
Aβ: 25R 23 24 25 25N 23-25
Lane: 1 2 3 4 5 6
SEC
215nm
280nm
13.7 kDa
6.5 kDa
6E10
JD1
4G8
6kDa
3kDa
Lane : 1 2 3 4 5 6 7 8
b
Control (PBS)
Aβ oligomers (JD1 + ve species)
%fEPSP Amplitude
Aβ / PBS
HFS
Time (min)
0.5mV
10ms
Compared LTP levels
% fEPSP amplitude (last 5min)
Control
Aβ
c
LTP recording
Protein extraction
Proteolysis
TMT-labelling
Off-Gel fractionation
LC-MS/MS
Proteome DB search
Bioinformatics
PRM
WB validation
d
Aβ / Ctrl
SMS
NFL
NLGN1
NEUG
BSN
SYUA
NEUM
SYUG
SYN1
VAMP2
SYUB
DLG4
HOME1
- Log10 (p-value)
Log2 Fold Change
e
DLG4
SYUA
NEUG
SMS
Aβ treated
control

**Figure 4. LMW oligomeric assemblies derived from C-terminally truncated Aβ species significantly inhibit LTP in the mouse hippocampus. a** left; representative DB screening of JD1 positive assemblies formed by the individual fragments Aβ23 to Aβ25 (lanes 2-5) as well as using a mixture of all fragments (lane 6). A reverse sequence of Aβ25-1 was used to show that aggregation of this sequence does not generate JD1 positive assemblies (lane 1). Right; SEC (Superdex 75, 10/300) and DB analysis of LMW assemblies formed by the mixture of Aβ fragments 1-23 to 1-25. JD1 positive assemblies were detected in SEC fraction volume 13ml, which contained dimeric and trimeric (≥6kDa) assemblies of these fragments (WB inset below), whereas monomers (≤3kDa) eluted in fraction volume 16ml. **b** Effect of application of LMW Aβ oligomers (SEC purified JD1 positive assemblies) on LTP in hippocampal slices from young wild type mice. Acute application of Aβ oligomers (500nM) to hippocampal slices significantly depressed LTP amplitude compared to control conditions (P<0.05). (inset right: top) Sample traces represent fEPSP before (**1**) and 60min after HFS (**2**) in control LTP, and before (**3**) and after HFS (**4**) Aβ-mediated LTP. (inset right: bottom) Bar chart comparing magnitude of LTP in control (190.6 ±22.94) and Aβ conditions (123.8 ±9.05) (N=5). All data are presented as Mean ±SEM and analyzed using unpaired Student's t-test. JD1 positive Aβ oligomer treated sliced (open circles) as compared to PBS controls (filled black circles). **c** Diagram of the analytical workflow applied for mouse hippocampal tissue extraction post-LTP recordings, protein digestion, isobaric labelling (TMT), off-gel isoelectric focusing, MS analysis and bioinformatics as well as orthogonal hit validation by targeted, quantitative MS and immuno-blotting. **d** Volcano plot analysis (y-axis of volcano plots: -Log10 p-value from two-sided T test corrected by Benjamini-Hochberg procedure) of differentially regulated proteins (x-axis: Log2 fold-change) in mouse brain tissue (n=3), following treatment with Aβ oligomers versus PBS controls. The dashed lines indicate a threshold of ± Log2 0.58 fold change (vertical lines) and a 0.05 p-value cut-off threshold (horizontal line). At the given cut-off, somatostatin (SMS) appears to be significantly up-regulated (FC= Log2 0.63) in Aβ treated brains. A similar trend in FC was observed for neurogranin (NEUG), however at significantly reduced level of significance (FC= log2 0.58). Proteins were graphed by fold change (FC, difference) and significance (-Log p) using a false discovery rate of 0.05 and an S0 of 0.1. Protein ID's in red (SMS and NEUG) were identified as significantly up-regulated (ggVolcanoR tool), whereas only SMS passed the confidence level of P<0.05 using Perseus software (Supplementary Data Figure 9). **e** Representative example of a regression analysis of (intra-TMT channel) protein correlation (mouse #2) for control versus Aβ treated brain tissue. A strong proteome correlation was observed for control versus Aβ treated tissues. As a reference, two protein markers with strong correlation between control and Aβ treated tissies are highlighted (DLG4 (PSD95) and SYUA protein). A clear correlation deviation was observed for the two synaptic markers SMS and NEUG.

To set out a strategic approach in assessing the acute neurotoxic properties of LMW oligomers, we decided to incubate mouse hippocampal brain slices with the above described, SEC purified JD1 positive assemblies, followed by *in vitro* electrophysiological recordings of long-term potentiation (LTP) in the Schaffer collateral commissural pathway of the CA1 region in mouse hippocampal slices. Brain slices were incubated with 500nM JD1 positive Aβ assemblies or an equal volume of PBS buffer (controls), followed by baseline recordings for 20min prior to high frequency stimulation (HFS) and LTP recording during 60min. LTP measurements were paired in a way, where control and Aβ treatment was carried out on hippocampal tissues derived from the same mouse brain.

Hippocampal tissues treated with these small oligomers resulted in a statistically significant reduction (123.8 ± 9.05, n=5) ($p \leq 0.01$) in LTP measured at 1hr post-HFS, when compared to matched controls (190.6 ±22.94, n=5, ) (Fig. 4b), which concurs with earlier reports showing an Aβ mediated attenuation of LTP *in vivo* and *in vitro* (5,17,18). IP-MS (JD1) analysis of the aCSF bath-solution showed that JD1 positive oligomers remained stable during the time course of LTP recordings (data not provided).

695 **LMW oligomers induce acute changes in somatostatin and neurogranin levels in the**
696 **mouse hippocampus.**
697 Following LTP recordings, brain slices from control and Aβ treated hippocampal tissues were
698 subjected to protein extraction, followed by downstream deep proteomic analysis to assess any
699 putative changes in synaptic markers following acute treatment with LMW Aβ assemblies. We
700 employed a relative quantitative proteomics approach using isobaric labelling with tandem-
701 mass-tags (TMT) followed by off-gel isoelectric focusing fractionation (IEF) (Fig. 4c), to study
702 the relative change in brain protein abundance and post-translational modifications (PTM) as a
703 result of acute Aβ treatment.
704 Deep proteomic analysis of mouse hippocampal tissues allowed for unbiased identification of
705 ≤5440 protein groups (FDR ≤1%) of which 6% of this proteome is associated with cellular
706 signalling mechanisms (Fig. 4d-e, Supplementary Data Fig. 6-8). Overall, extended
707 bioinformatics analysis of the mouse brain proteome did not reveal major changes in protein
708 abundances in control versus Aβ treated tissues (Fig. 4d-e and Supplementary Data Fig. 9). This
709 observation is in agreement with the general knowledge that *de novo* protein synthesis is mainly
710 associated with late-phase LTP, consisting of several hours or days (38). We nevertheless found
711 a statistically significant fold-change (-Log p = 2.84) of the pre-synaptic protein somatostatin
712 (SMS) following Aβ treatment (Fig. 4d-e and Supplementary Data Fig. 9a&b). Interestingly,
713 rapid hippocampal SMS release has been associated with acute stress in animals (39) and
714 somatostatin is known to play a key role in regulating Aβ metabolism through modulating
715 proteolytic degradation by neprilysin (40).
716 Next, a functional protein partnership search was carried out using the STRING database for
717 the integration of both, known and predicted protein-protein interaction networks (physical or
718 functional) to identify potential somatostatin interaction networks (Fig. 5a-b and
719 Supplementary Data Fig. 8a-b). Active somatostatin interaction was found for the protein
720 neurogranin (Neug / Nrgn), a well-established marker of neurodegeneration (41,42), whereas
721 neurogranin itself appears to form a network hub with different pre- and post-synaptic markers
722 (Fig. 5b). Bioinformatics analysis revealed a small fold change (Log2 fold change = 0.58) for
723 NEUG in Aβ treated tissue, however, this marker failed to show statistical significance (-Log p
724 = 1.34) (Fig. 4d-e). The small change in NEUG levels following Aβ treatment is an intriguing
725 observation because neurogranin expression is known to be regulated by synaptic activity (43)
726 and memory encoding requires a rapid (≤ 15min) *de novo* synthesis of neurogranin in the mouse
727 hippocampus (44). Moreover, neurogranin is known to play a key role in the regulation of

metaplasticity, by lowering the threshold for LTP induction (45) and the Aβ oligomer induced inhibitory effect on LTP can be reversed by increasing neurogranin levels (46).

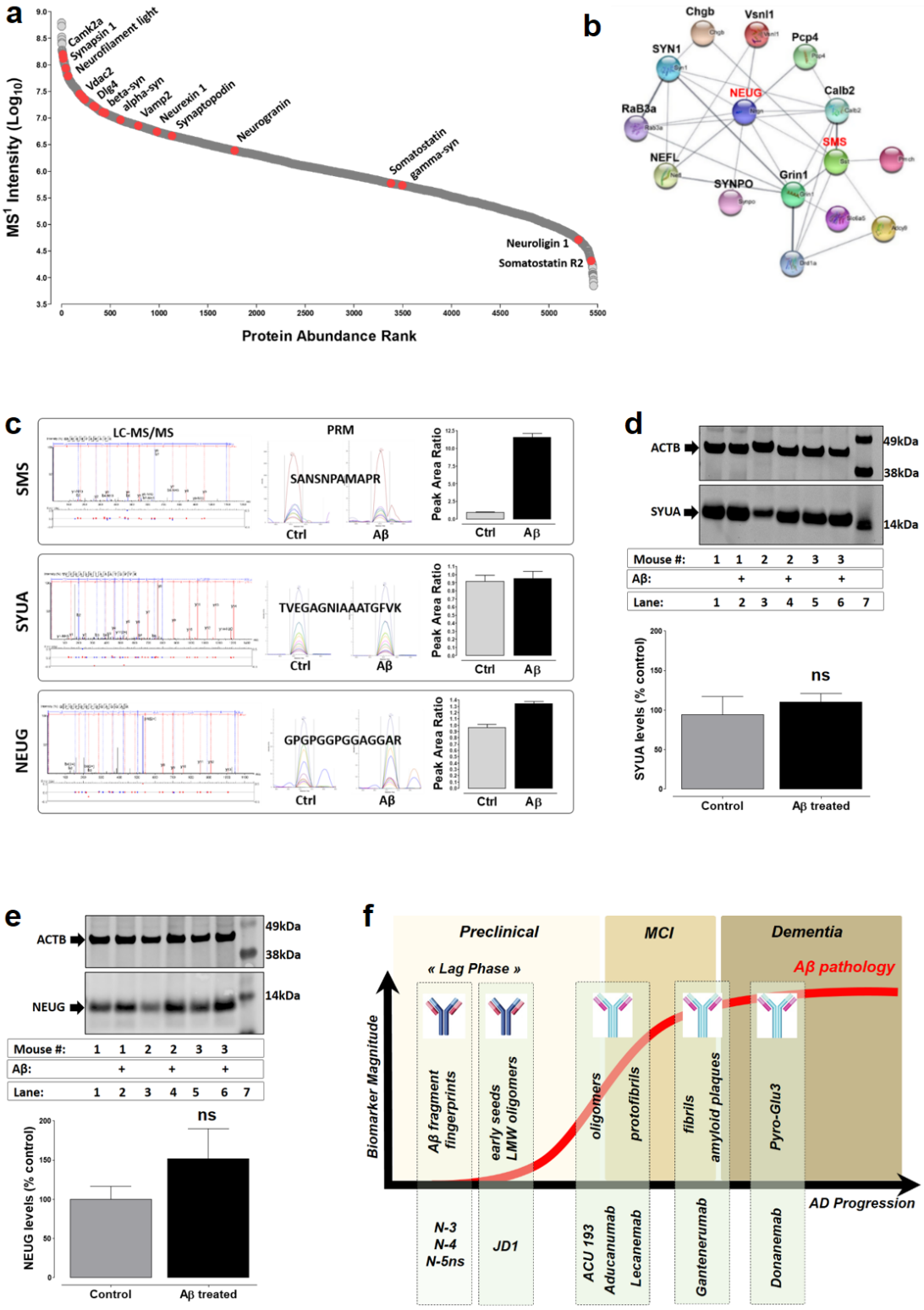

**Figure 5. Acute Aβ neurotoxicity induces rapid changes in somatostatin and neurogranin levels in the mouse hippocampus. a** Protein abundance analysis showing the relative abundance of different pre- and post-synaptic markers highlighted in red. **b** Selected zoom of the protein association network analysis (STRING), centred on neurograning (Neug) protein and showing an interaction with somatostatin (SMS) protein as well as a network with other proteins. (see Supplementary Data Fig. 8 for larger interaction network). **c** Summary of label-free, quantitative MS of the pre- and post-synaptic markers: somatostatin, alpha-synuclein and neurogranin (from top to bottom). Left; $MS^2$ spectra of one proteotypic peptide monitored for SMS, SYUA and NEUG protein. Centre; $MS^2$ fragment areas of selected $MS^2$ transitions. Right; calculated relative protein areas derived from quantitative MS analysis. **d** Orthogonal validation of SYUA levels found in Aβ treated (lanes: 2, 4 & 6) and control (lanes: 1, 3 & 5) brain tissue. (lane 7: MWM) using WB. Below; Summary of actin normalized (ACTB) densitometry analysis of NEUG levels detected in Aβ treated (110.3±10, mean ± SD, n=3) versus control (94.3±23) (p=0.489, t-test, two-tailed) animals. (ns: not significant). **e** Orthogonal validation of NEUG levels found in Aβ treated (lanes: 2, 4 & 6) and control (lanes: 1, 3 & 5) brain tissue. (lane 7: MWM) using WB. Below; Summary of actin normalized (ACTB) densitometry analysis of NEUG levels detected in Aβ treated (152±38, mean ± SD, n=3) versus control (100±16.5) (p=0.082, t-test, two-tailed) animals. (ns: not significant). **f** Summary of neo-epitope (N3, N4 & N5ns) and JD1 antibody binding features, as well as earlier reported binding properties of different clinical antibodies. The diagram depicts a perspective of the current understanding of the pathological accumulation of Aβ assemblies (morphologies) and antibody molecules against these different Aβ entities: oligomers (ACU 193, aducanumab) and protofibrils (lecanemab), fibrils or amyloid plaques (gantenerumab, aducanumab) or modifications (pyro-E3) found within the N-terminal region of Aβ (donanemab). The combination of both, neo-epitope and JD1 antibodies may allow early interception of small oligomeric species prior to the accumulation of larger Aβ assemblies.

To confirm the significance of the differentially regulated levels found for somatostatin and neurogranin, we decided to analyse the abundance of these two synaptic markers using a targeted, quantitative MS approach known as Parallel Reaction Monitoring (PRM), which allows unbiased identification of low abundant species in complex sample matrices. Quantitative MS analysis revealed that, levels of SMS were indeed significantly increased in Aβ treated mouse brains when compared to control brain slices. Similarly, NEUG levels where approximately ≥ 30% increased in Aβ treated brains, whereas levels of the predominantly found presynaptic marker α-synuclein (SYUA) did not differ between both groups (Fig. 5c and Supplementary Data Fig. 9b&c). Orthogonal validation by WB of the pre- and postsynaptic markers of SYUA (Fig. 5d) and NEUG respectively (Fig. 5e), as well as homer1 and post-synaptic density protein (PSD95 / Dlg4) (Supplementary Data Fig. 9c), further corroborate the findings by MS. However, immuno-blot detection of the small, presynaptic protein somatostatin proved to be challenging (Supplementary Data Fig. 9c) and therefore highlights the advantage of implementing targeted and quantitative MS assays, for an unbiased identification and quantification of scarce proteins (Supplementary Data Fig. 10).

775 **Aβ oligomer mediated changes in mouse hippocampal phospho-proteome.**
776 It has been well established that Aβ accelerates hyperphosphorylation of tau protein, which in
777 turn aggravates neuronal tauopathy (47). We therefore sought to identify putative changes in
778 site-specific protein phosphorylation, as a result of acute Aβ treatment, using a titanium-dioxide
779 ($TiO_2$) bead enabled phospho-peptide enrichment approach, followed by LC-MS analysis.
780 Overall, phospho-enrichment analysis allowed the identification of ≥7800 phospho-sites (FDR
781 ≤1%), in control and Aβ treated hippocampal slices. Our target proteins of interest were
782 primarily focused on well-established markers of synaptic plasticity, as well as proteins that
783 have previously been reported to be susceptible to phosphorylation as a result of Aβ toxicity
784 (48). Phospho-proteomic analysis revealed differential levels of site-specific phosphorylation
785 of the calcium/calmodulin dependent protein kinase II alpha (CAMKIIa) protein, post-synaptic
786 density protein (PSD95 / Dlg4), synapsin 1 & 2 (SYN1 & SYN2), synaptophysin (SYPH) as
787 well as tau (TAU) protein in control versus Aβ treated brains (Supplementary Data Table II).
788 In spite of the here reported MS identification of some differentially modified tau species found
789 in acute Aβ treated brains, we were not able to confirm earlier reported tau phosphorylation *in*
790 *vitro* at residues pS202 or pS416 using structurally different Aβ assemblies (49).
791 Collectively, our deep proteomic and phospho-proteomic analysis may further shed light on the
792 acute Aβ mediated effects on synaptic plasticity. The observed, differentially regulated synaptic
793 protein somatostatin and, to some extent neurogranin, is intriguing, and clearly merits a more
794 thorough investigation in the future but is beyond the scope of the current study.
795
796
797 **Discussion:**
798 In this study, we provide analytical insight into the composition of LMW Aβ oligomers. We
799 show that small Aβ assemblies of putative dimeric, trimeric and tetrameric nature consist of a
800 combination of full-length Aβ42 as well as a repertoire of C-terminally truncated Aβ species,
801 of which the latter may also independently seed to form SDS-stable, HMW oligomeric
802 assemblies of 50kDa-200kDa mass range. Our unbiased MS identification of identical Aβ
803 fragment fingerprints, together with the JD1 positive assemblies detected in post-mortem AD
804 brains, further highlights the pathological significance of Aβ fragments; Aβ1-23 to Aβ1-25.
805 Generally, our findings allow to draw strong parallels with earlier reported observations of
806 typical Aβ fragment fingerprints (12) as well as the detection of a repertoire of different N- and,
807 C-terminally truncated Aβ species in human CSF samples (36,49,50). The independent report
808 of specific Aβ fragments found in human post-mortem AD brains as well as Down-syndrome

809 (DS) subjects (51,52) further corroborates the significance of the findings reported here.
810 Nevertheless, it remains to be confirmed, if the here reported key findings mirror earlier reports
811 on the inhibition of LTP, using similar LMW oligomeric assemblies (22) or, soluble ~7kDa Aβ
812 species isolated from post-mortem AD brains (9,10,15).
813 We provide compelling analytical proof, that the application of our recently developed neo-
814 epitope antibodies against different truncated Aβ isoforms allows for a highly selective pull-
815 down (IP) of SDS-PAGE stable assemblies from human post-mortem AD brains. These
816 isolated Aβ assemblies strongly resemble the LMW Aβ species (4-7kDa) typically found
817 following IP of formic acid induced dissociation of ADDLs. Our findings are in strong
818 agreement with earlier reports indicating, that LMW Aβ oligomers consist of a repertoire of
819 truncated Aβ species and full-length Aβ42 or Aβ40 (16,53). However, earlier analytical
820 attempts in identifying specific Aβ isoforms associated with LWM Aβ assemblies and, more
821 specifically, the ~4kDa and ~7kDa Aβ species, have failed (16).
822 The lack in scientific and clinical consensus on the therapeutic efficacy of some clinical
823 antibodies as well as the ongoing, heated debate on viable, oligomeric Aβ targets (54) (55),
824 emphasizes the strong need for identifying highly specific Aβ targets for the development of
825 next generation disease modifying-therapies. Recent studies corroborate the notion, that
826 therapeutically targetable Aβ seeds exist during the lag phase of protein aggregation, and that
827 acute administration of aducanumab in young mice led to a significant reduction of Aβ
828 pathology in the mouse brain (1). Therefore, a successful clinical translation of specific Aβ
829 target hotspots will allow a therapeutic interception of early Aβ seeds during the long, insidious
830 lag phase of AD and prior to the accumulation of larger, metastable Aβ assemblies of
831 protofibrillar or fibrillar nature (Fig. 5f). Improving antibody-binding properties for small Aβ
832 assemblies may allow a selective targeting of early, pathological Aβ seeds during disease onset
833 and therefore attenuate or even prevent the progression to severe dementia. The here reported
834 monoclonal antibody binding features observed with JD1 represents a first example of a new
835 class of future antibody molecules.
836 Our understanding of JD1 binding properties give rise to important Aβ target "loopholes"
837 associated with earlier developed anti-conformational antibodies. Yet, it remains to be
838 determined, if other antibody molecules, such as the anti-oligomer ACU 193 (3) or anti-
839 protofibril antibody lecanemab, currently undergoing clinical validation (56,57), provide
840 similar binding properties for the here described LMW Aβ assemblies. Our observation on
841 aducanumab's decreased binding affinity for LMW oligomeric assemblies has not been
842 reported before, and this finding is somehow surprising, because aducanumab's binding epitope

843 is known to span the N-terminal region of residues 3-6. Preferential aducanumab binding was
844 reported for oligomeric and fibrillar Aβ species derived from full-length Aβ42 peptide (29),
845 whereas oligomers derived from the N-terminally truncated forms of Aβ 5-42 to Aβ11-42 were
846 no longer detected with aducanumab (58). It is conceivable, that the strong seeding propensity
847 observed with fragments Aβ1-23, Aβ1-24 and Aβ1-25, as well as the C-terminally amidated
848 forms of these fragments, involves rapid conformational changes associated with the amyloid
849 driving segment of residues 16-25 and that JD1 binding is associated with a unique
850 conformational structure found within this Aβ segment. Discrepancies in aducanumab binding
851 properties have been previously observed, following immunization of a transgenic mouse
852 model of AD, resulting in a clear reduction in amyloid plaques but a failure in clearance of
853 vascular amyloid (CAA) (1,29). Interestingly, it was reported that the deposition of specific Aβ
854 isoforms appears to differ in subjects with vascular dementia, when compared with AD patients
855 (51), which is in line with the positive immuno-staining found for fragment Aβ1-25 in CAA
856 subjects (12).
857 Significant IHC staining of Aβ oligomers was reported using different conformation specific
858 antibodies (3) with binding properties against large (≥80kDa) Aβ assemblies (59). The lack in
859 JD1 staining of amyloid plaques may not appear surprising, given JD1's binding specificity for
860 LMW Aβ assemblies and the overall scarcity of Aβ oligomers reported in the human brain,
861 which is an observation also made by others using different anti-oligomer antibodies (3,28,61).
862 Nevertheless, our high-resolution array tomography clearly shows co-localization of JD1
863 positive species at post-synaptic terminals, which is in line with earlier reports, using different
864 conformational specific antibodies (34).
865 Taken together, the selective binding profile found with JD1 could be a beneficial antibody
866 feature, by decreasing the risk of dose-limiting side effects associated with passive
867 immunization, as well as increasing the antibody's bioavailability for rather early, neurotoxic
868 oligomeric assemblies (61). Overall, the here reported binding properties of JD1 highlights the
869 importance in further improving and developing novel antibody tools, with high target
870 selectivity for small, pathological Aβ seeds or oligomeric entities derived thereof. To date, the
871 development of highly specific anti-oligomeric antibodies remains a strong unmet medical need
872 for future disease-modifying therapeutics in AD. Improvement of immuno-based target
873 selectivity for acute, pathological Aβ species will inevitably provide early insight into the
874 disease pathology. This in turn will serve as an indispensable diagnostic tool for evaluation of
875 disease onset and progression, prior to the accumulation of clinical targets associated with pyro-

$Glu_3$ modification (Donanemab) (61) or large Aβ assemblies of protofibrilar (lecanemab) (57) and fibrillar structure (gantenerumab) (56) (Fig. 5f).

Monitoring changes in CSF and plasma Aβ42/40 ratios, as well as detection of early Aβ seeds, together with other, clinically well-established biomarkers of neurodegeneration (e.g. p-Tau, Nfl, Ngrn), may overall improve the diagnostic accuracy for individuals suffering from mild cognitive impairment, who may benefit from early therapeutic intervention with future disease modifying therapies. This could help to attenuate the pathological progression to severe dementia and overall improve the quality of life in patients in the long run.

910 **References**

911

912 1. Uhlmann RE, Rother C, Rasmussen J, Schelle J, Bergmann C, Ullrich Gavilanes EM, et al.
913 Acute targeting of pre-amyloid seeds in transgenic mice reduces Alzheimer-like pathology
914 later in life. Nat Neurosci. 2020 Dec;23(12):1580–8.
915 2. Selkoe DJ. Soluble oligomers of the amyloid β-protein impair synaptic plasticity and
916 behavior. Behavioural Brain Research. 2008 Sep;192(1):106–13.
917 3. Viola KL, Bicca MA, Bebenek AM, Kranz DL, Nandwana V, Waters EA, et al. The
918 Therapeutic and Diagnostic Potential of Amyloid β Oligomers Selective Antibodies to Treat
919 Alzheimer's Disease. Front Neurosci. 2022 Jan 3;15:768646.
920 4. Glabe CG. Structural Classification of Toxic Amyloid Oligomers. Journal of Biological
921 Chemistry. 2008 Oct;283(44):29639–43.
922 5. Walsh DM, Klyubin I, Fadeeva JV, Cullen WK, Anwyl R, Wolfe MS, et al. Naturally
923 secreted oligomers of amyloid b protein potently inhibit hippocampal long-term potentiation
924 in vivo. 2002;416:5.
925 6. Liu P, Reed MN, Kotilinek LA, Grant MKO, Forster CL, Qiang W, et al. Quaternary
926 Structure Defines a Large Class of Amyloid-β Oligomers Neutralized by Sequestration. Cell
927 Reports. 2015 Jun;11(11):1760–71.
928 7. Cerf E, Sarroukh R, Tamamizu-Kato S, Breydo L, Derclaye S, Dufrêne YF, et al.
929 Antiparallel β-sheet: a signature structure of the oligomeric amyloid β-peptide. Biochemical
930 Journal. 2009 Aug 1;421(3):415–23.
931 8. Gu L, Liu C, Stroud JC, Ngo S, Jiang L, Guo Z. Antiparallel Triple-strand Architecture for
932 Prefibrillar Aβ42 Oligomers. Journal of Biological Chemistry. 2014 Sep;289(39):27300–13.
933 9. Yang T, Li S, Xu H, Walsh DM, Selkoe DJ. Large Soluble Oligomers of Amyloid β-Protein
934 from Alzheimer Brain Are Far Less Neuroactive Than the Smaller Oligomers to Which They
935 Dissociate. J Neurosci. 2017 Jan 4;37(1):152–63.

936 10. Shankar GM, Li S, Mehta TH, Garcia-Munoz A, Shepardson NE, Smith I, et al.
937 Amyloid-β protein dimers isolated directly from Alzheimer's brains impair synaptic
938 plasticity and memory. Nat Med. 2008 Aug;14(8):837–42.
939 11. Lesné S, Koh MT, Kotilinek L, Kayed R, Glabe CG, Yang A, et al. A specific amyloid-
940 β protein assembly in the brain impairs memory. Nature. 2006 Mar;440(7082):352–7.
941 12. Rudinskiy N, Fuerer C, Demurtas D, Zamorano S, De Piano C, Herrmann AG, et al.
942 Amyloid-beta oligomerization is associated with the generation of a typical peptide fragment
943 fingerprint. Alzheimer's & Dementia. 2016 Sep;12(9):996–1013.
944 13. O'Nuallain B, Freir DB, Nicoll AJ, Risse E, Ferguson N, Herron CE, et al. Amyloid -
945 Protein Dimers Rapidly Form Stable Synaptotoxic Protofibrils. Journal of Neuroscience.
946 2010 Oct 27;30(43):14411–9.
947 14. Klyubin I, Betts V, Welzel AT, Blennow K, Zetterberg H, Wallin A, et al. Amyloid
948 Protein Dimer-Containing Human CSF Disrupts Synaptic Plasticity: Prevention by Systemic
949 Passive Immunization. Journal of Neuroscience. 2008 Apr 16;28(16):4231–7.
950 15. Mc Donald JM, O'Malley TT, Liu W, Mably AJ, Brinkmalm G, Portelius E, et al. The
951 aqueous phase of Alzheimer's disease brain contains assemblies built from ∼4 and ∼7 kDa
952 Aβ species. Alzheimer's & Dementia. 2015 Nov;11(11):1286–305.
953 16. Brinkmalm G, Hong W, Wang Z, Liu W, O'Malley TT, Sun X, et al. Identification of
954 neurotoxic cross-linked amyloid-b dimers in the Alzheimer's brain. :17.
955 17. Freir DB, Holscher C, Herron CE. Blockade of Long-Term Potentiation by β-Amyloid
956 Peptides in the CA1 Region of the Rat Hippocampus In Vivo. Journal of Neurophysiology.
957 2001 Feb 1;85(2):708–13.
958 18. Schmid AW, Freir DB, Herron CE. Inhibition of LTP in vivo by beta-amyloid peptide
959 in different conformational states. Brain Research. 2008 Mar;1197:135–42.

960 19. Freir DB, Herron CE. Nicotine Enhances the Depressive Actions of Aβ $_{1–40}$ on Long-
961 Term Potentiation in the Rat Hippocampal CA1 Region In Vivo. Journal of
962 Neurophysiology. 2003 Jun;89(6):2917–22.
963 20. McIntee FL, Giannoni P, Blais S, Sommer G, Neubert TA, Rostagno A, et al. In vivo
964 Differential Brain Clearance and Catabolism of Monomeric and Oligomeric Alzheimer's Aβ
965 protein. Front Aging Neurosci [Internet]. 2016 Sep 27 [cited 2020 Apr 7];8. Available from:
966 http://journal.frontiersin.org/Article/10.3389/fnagi.2016.00223/abstract
967 21. Mazzitelli S, Filipello F, Rasile M, Lauranzano E, Starvaggi-Cucuzza C, Tamborini M,
968 et al. Amyloid-β 1–24 C-terminal truncated fragment promotes amyloid-β 1–42 aggregate
969 formation in the healthy brain. acta neuropathol commun. 2016 Dec;4(1):110.
970 22. Lambert MP, Klein WL. Diffusible, nonfibrillar ligands derived from Abeta1-42 are
971 potent central nervous system neurotoxins. Proc Natl Acad Sci USA. 1998 May;
972 23. Velasco PT, Heffern MC, Sebollela A, Popova IA, Lacor PN, Lee KB, et al. Synapse-
973 Binding Subpopulations of Aβ Oligomers Sensitive to Peptide Assembly Blockers and scFv
974 Antibodies. ACS Chem Neurosci. 2012 Nov 21;3(11):972–81.
975 24. Sorrentino V, Romani M, Mouchiroud L, Beck JS, Zhang H, D'Amico D, et al.
976 Enhancing mitochondrial proteostasis reduces amyloid-β proteotoxicity. Nature. 2017
977 Dec;552(7684):187–93.
978 25. Rudinskiy et al. - 2016 - Amyloid-beta oligomerization is associated with th.pdf.
979 26. Kayed R, Head E, Sarsoza F, Saing T, Cotman CW, Necula M, et al. Fibril specific,
980 conformation dependent antibodies recognize a generic epitope common to amyloid fibrils
981 and fibrillar oligomers that is absent in prefibrillar oligomers. Mol Neurodegeneration. 2007
982 Dec;2(1):18.

983 27. Kayed R, Canto I, Breydo L, Rasool S, Lukacsovich T, Wu J, et al. Conformation
984 dependent monoclonal antibodies distinguish different replicating strains or conformers of
985 prefibrillar Aβ oligomers. Mol Neurodegeneration. 2010 Dec;5(1):57.
986 28. Gibbs E, Silverman JM, Zhao B, Peng X, Wang J, Wellington CL, et al. A Rationally
987 Designed Humanized Antibody Selective for Amyloid Beta Oligomers in Alzheimer's
988 Disease. Sci Rep. 2019 Dec;9(1):9870.
989 29. Sevigny J, Chiao P, Bussière T, Weinreb PH, Williams L, Maier M, et al. The antibody
990 aducanumab reduces Aβ plaques in Alzheimer's disease. Nature. 2016 Sep 1;537(7618):50–
991 6.
992 30. Ladiwala ARA, Litt J, Kane RS, Aucoin DS, Smith SO, Ranjan S, et al. Conformational
993 Differences between Two Amyloid β Oligomers of Similar Size and Dissimilar Toxicity. J
994 Biol Chem. 2012 Jul 13;287(29):24765–73.
995 31. Britschgi M, Olin CE, Johns HT, Takeda-Uchimura Y, LeMieux MC, Rufibach K, et
996 al. Neuroprotective natural antibodies to assemblies of amyloidogenic peptides decrease with
997 normal aging and advancing Alzheimer's disease. Proc Natl Acad Sci USA. 2009 Jul
998 21;106(29):12145–50.
999 32. Klaver AC, Finke JM, Digambaranath J, Balasubramaniam M, Loeffler DA. Antibody
1000 concentrations to Aβ1–42 monomer and soluble oligomers in untreated and antibody–
1001 antigen-dissociated intravenous immunoglobulin preparations. International
1002 Immunopharmacology. 2010 Jan;10(1):115–9.
1003 33. Magga J, Puli L, Pihlaja R, Kanninen K, Neulamaa S, Malm T, et al. Human intravenous
1004 immunoglobulin provides protection against Ab toxicity by multiple mechanisms in a mouse
1005 model of Alzheimer's disease. 2010;15.

1006 34. Pickett EK, Koffie RM, Wegmann S, Henstridge CM, Herrmann AG, Colom-Cadena
1007 M, et al. Non-Fibrillar Oligomeric Amyloid-β within Synapses. Stranahan A, editor. JAD.
1008 2016 Aug 3;53(3):787–800.
1009 35. Petersen RC, Smith GE, Waring SC, Ivnik RJ, Tangalos EG, Kokmen E. Mild Cognitive
1010 Impairment: Clinical Characterization and Outcome. Arch Neurol. 1999 Mar 1;56(3):303.
1011 36. Portelius E, Andreasson U, Ringman JM, Buerger K, Daborg J, Buchhave P, et al.
1012 Distinct cerebrospinal fluid amyloid β peptide signatures in sporadic and PSEN1 A431E-
1013 associated familial Alzheimer's disease. Mol Neurodegeneration. 2010;5(1):2.
1014 37. Hebbar S, Lee E, Manna M, Steinert S, Kumar GS, Wenk M, et al. A fluorescent
1015 sphingolipid binding domain peptide probe interacts with sphingolipids and cholesterol-
1016 dependent raft domains. Journal of Lipid Research. 2008 May;49(5):1077–89.
1017 38. Younts TJ, Monday HR, Dudok B, Klein ME, Jordan BA, Katona I, et al. Presynaptic
1018 Protein Synthesis Is Required for Long-Term Plasticity of GABA Release. Neuron. 2016
1019 Oct;92(2):479–92.
1020 39. Arancibia S, Payet O, Givalois L, Tapia-Arancibia L. Acute stress and dexamethasone
1021 rapidly increase hippocampal somatostatin synthesis and release from the dentate gyrus
1022 hilus. Hippocampus. 2001;11(4):469–77.
1023 40. Saito T, Iwata N, Tsubuki S, Takaki Y, Takano J, Huang SM, et al. Somatostatin
1024 regulates brain amyloid β peptide Aβ42 through modulation of proteolytic degradation. Nat
1025 Med. 2005 Apr;11(4):434–9.
1026 41. Hesse R, Hurtado ML, Jackson RJ, Eaton SL, Herrmann AG, Colom-Cadena M, et al.
1027 Comparative profiling of the synaptic proteome from Alzheimer's disease patients with
1028 focus on the APOE genotype. acta neuropathol commun. 2019 Dec;7(1):214.

1029 42. Wellington H, Paterson RW, Portelius E, Törnqvist U, Magdalinou N, Fox NC, et al.
1030 Increased CSF neurogranin concentration is specific to Alzheimer disease. Neurology. 2016
1031 Mar 1;86(9):829–35.
1032 43. Garrido-García A, de Andrés R, Jiménez-Pompa A, Soriano P, Sanz-Fuentes D,
1033 Martínez-Blanco E, et al. Neurogranin Expression Is Regulated by Synaptic Activity and
1034 Promotes Synaptogenesis in Cultured Hippocampal Neurons. Mol Neurobiol. 2019
1035 Nov;56(11):7321–37.
1036 44. Jones KJ, Templet S, Zemoura K, Kuzniewska B, Pena FX, Hwang H, et al. Rapid,
1037 experience-dependent translation of neurogranin enables memory encoding. Proc Natl Acad
1038 Sci USA. 2018 Jun 19;115(25):E5805–14.
1039 45. Zhong L, Gerges NZ. Neurogranin Regulates Metaplasticity. Front Mol Neurosci. 2020
1040 Jan 24;12:322.
1041 46. Kaleka KS, Gerges NZ. Neurogranin restores amyloid β-mediated synaptic transmission
1042 and long-term potentiation deficits. Experimental Neurology. 2016 Mar;277:115–23.
1043 47. Terwel D, Muyllaert D, Dewachter I, Borghgraef P, Croes S, Devijver H, et al. Amyloid
1044 Activates GSK-3β to Aggravate Neuronal Tauopathy in Bigenic Mice. The American
1045 Journal of Pathology. 2008 Mar;172(3):786–98.
1046 48. Jin M, Shepardson N, Yang T, Chen G, Walsh D, Selkoe DJ. Soluble amyloid β-protein
1047 dimers isolated from Alzheimer cortex directly induce Tau hyperphosphorylation and
1048 neuritic degeneration. Proc Natl Acad Sci USA. 2011 Apr 5;108(14):5819–24.
1049 49. Amar F, Sherman MA, Rush T, Larson M, Boyle G, Chang L, et al. The amyloid-β
1050 oligomer Aβ*56 induces specific alterations in neuronal signaling that lead to tau
1051 phosphorylation and aggregation. Sci Signal. 2017 May 9;10(478):eaal2021.

1052 50. Bibl M, Gallus M, Welge V, Esselmann H, Wiltfang J. Aminoterminally Truncated and
1053 Oxidized Amyloid-β Peptides in the Cerebrospinal Fluid of Alzheimer's Disease Patients.
1054 JAD. 2012 Apr 16;29(4):809–16.
1055 51. Larner AJ. Hypothesis: amyloid NL-peptides truncated at the N-terminus contribute to
1056 the pathogenesis of Alzheimer's disease. Neurobiology of Aging. 1999;5.
1057 52. Gkanatsiou E, Portelius E, Toomey CE, Blennow K, Zetterberg H, Lashley T, et al. A
1058 distinct brain beta amyloid signature in cerebral amyloid angiopathy compared to
1059 Alzheimer's disease. Neuroscience Letters. 2019 May;701:125–31.
1060 53. Gkanatsiou E, Sahlin C, Portelius E, Johannesson M, Söderberg L, Fälting J, et al.
1061 Characterization of monomeric and soluble aggregated Aβ in Down's syndrome and
1062 Alzheimer's disease brains. Neuroscience Letters. 2021 May;754:135894.
1063 54. Hong W, Wang Z, Liu W, O'Malley TT, Jin M, Willem M, et al. Diffusible, highly
1064 bioactive oligomers represent a critical minority of soluble Aβ in Alzheimer's disease brain.
1065 Acta Neuropathol. 2018 Jul;136(1):19–40.
1066 55. Benilova I, Karran E, De Strooper B. The toxic Aβ oligomer and Alzheimer's disease:
1067 an emperor in need of clothes. Nat Neurosci. 2012 Mar;15(3):349–57.
1068 56. Ashe. Alzheimer's target still viable but untested.
1069 57. Bohrmann B, Baumann K, Benz J, Gerber F, Huber W, Knoflach F, et al.
1070 Gantenerumab: A Novel Human Anti-Aβ Antibody Demonstrates Sustained Cerebral
1071 Amyloid-β Binding and Elicits Cell-Mediated Removal of Human Amyloid-β. JAD. 2012
1072 Jan 12;28(1):49–69.
1073 58. Sehlin D, Englund H, Simu B, Karlsson M, Ingelsson M, Nikolajeff F, et al. Large
1074 Aggregates Are the Major Soluble Aβ Species in AD Brain Fractionated with Density
1075 Gradient Ultracentrifugation. Bush AI, editor. PLoS ONE. 2012 Feb 15;7(2):e32014.

1076 59. Desai AA, Smith MD, Zhang Y, Makowski EK, Gerson JE, Ionescu E, et al. Rational
1077 affinity maturation of anti-amyloid antibodies with high conformational and sequence
1078 specificity. Journal of Biological Chemistry. 2021 Jan;296:100508.
1079 60. Sebollela A, Mustata GM, Luo K, Velasco PT, Viola KL, Cline EN, et al. Elucidating
1080 Molecular Mass and Shape of a Neurotoxic Aβ Oligomer. ACS Chem Neurosci. 2014;8.
1081 61. Bakrania P, Hall G, Bouter Y, Bouter C, Beindorff N, Cowan R, et al. Discovery of a
1082 novel pseudo β-hairpin structure of N-truncated amyloid-β for use as a vaccine against
1083 Alzheimer's disease. Mol Psychiatry [Internet]. 2021 Nov 15 [cited 2022 Apr 6]; Available
1084 from: https://www.nature.com/articles/s41380-021-01385-7
1085 62. Cynis H, Frost JL, Crehan H, Lemere CA. Immunotherapy targeting pyroglutamate-3
1086 Aβ: prospects and challenges. Mol Neurodegeneration. 2016 Dec;11(1):48.
1087 63. Metais C, Brennan K, Mably AJ, Scott M, Walsh DM, Herron CE. Simvastatin
1088 Treatment Preserves Synaptic Plasticity in $A_{NL}$PPswe/PS1dE9 Mice. C Me. :15.
1089 64. Hughes B, Herron CE. Cannabidiol Reverses Deficits in Hippocampal LTP in a Model
1090 of Alzheimer's Disease. Neurochem Res. 2019 Mar;44(3):703–13.

1091
1092
1093
1094
1095
1096

1097 **Materials and Methods:**

1098

1099 **Aβ peptide preparation.**

1100 Full-length wild type (wt) Aβ peptides Aβ1-40 and Aβ1-42 Aβ (BACHEM, Switzerland) were
1101 dissolved in 1,1,1,3,3,3-Hexafluoro-2-propanol (HFIP) at a concentration of 1mg/ml, followed
1102 by a 10-min sonication to break any preformed aggregates. HFIP solution was evaporated
1103 under a ventilated fume hood by applying a light stream of $N_2$ gas. The HFIP film containing

1104 the Aβ peptide was either directly re-suspended in 100% DMSO and further diluted to 1%
1105 DMSO in a new buffer or stored dry at −80 °C until use. Aβ peptide fragments comprising of
1106 residues: 1-23, 1-24-$NH_2$, 1-25, 1-25-$NH_2$ (purity of ≥ 97%) were purchased from GenicBio
1107 Ltd. (Shanghai, China) and Aβ1-42 and Aβ1-40 were purchased from Bachem
1108 (Schwitzerland), Aβ40-Arc was kindly provided by Prof. Hilal Lashuel (EPFL) and reverse
1109 peptide Aβ42-1 was kindly provided by Prof. Gräff (EPFL). Recombinant alpha-synuclein
1110 protein was a gift from rPeptide (GA, USA).
1111
1112 **In vitro Aβ peptide aggregation studies.**
1113 Aggregation kinetics were carried out as reported by (Ladiwala et al.). Briefly, HFIP dried Aβ
1114 peptide films were solubilized in 50mM NaOH, sonicated and further diluted to 5mM with
1115 PBS (or 30mM Tris, 150mM NaCl) to a final Aβ concentration of 0.05-0.1 mg/ml for truncated
1116 Aβ fragments and full-length peptides of Aβ1-40, 0.1 mg/ml mutant Aβ1-40 Arc, and 0.05
1117 mg/ml Aβ1-42. Aβ preparations were then centrifuged (22,000 x g) for 30min at 4°C and the
1118 supernatant (90-95% volume) was recovered and transferred into a new Eppendorf tube.
1119 Supernatant samples were then incubated at 37°C and left for spontaneous aggregation during
1120 either 0-20 hrs (short-term) or 1-5 days (intermediate). Aggregated sample aliquots were drawn
1121 at different time points and either analyzed immediately using MS and/or DB or snap frozen
1122 in liquid nitrogen and stored at -80°C. Typically, one microliter was spotted onto a
1123 nitrocellulose membrane for dotblotting (corresponding to either 25, 50ng to100ng / spot) or
1124 mixed with alpha-cyano matrix for MALDI-TOF/TOF analysis.
1125
1126 **Digestion of Aβ peptides.**
1127 Proteolytic digestion using LysN (2ng/ul) was performed overnight at 37 °C in 50 mM
1128 ammonium bicarbonate, pH 10 (LysN buffer). For in-gel digestions, peptides were extracted
1129 from gels and concentrated by Speed-Vacuum prior to LC-MS/MS measurements.
1130 Immunoprecipitated samples (IP), were reduced and alkylated followed by in-solution
1131 digestion at 37°C using standard LysN buffer (50ul) and approximately 70ng of LysN. Dried
1132 samples were resuspended in 5% DMSO and 2.5% FA followed by LC-MS/MS, LC-MRM
1133 and PRM analysis.
1134
1135 **Matrix assisted Laser Desorption/Ionization Time-of-flight Mass Spectrometry (MALDI**
1136 **TOF/TOF).**

1137 Aliquots (2 µl) of samples were used for MALDI-TOF/TOF MS (ABI 4800 model, Applied
1138 Biosystems) measurements. Matrix solution of α-cyano-4-hydroxycinnamic acid (7 mg/ml in
1139 ACN/0.1% TFA (1:1, v/v)) was used for sample deposition. The sample (1 µl) was mixed with
1140 1 µl of matrix solution and then 1 µl of this mixture was deposited in duplicates on the target
1141 plate and allowed to air dry. Samples were analyzed in reflectron positive mode.
1142
1143 **Sandwich ELISA for detection of Aβ oligomers**
1144 JD1 antibody was adsorbed to high protein binding Nunc-Immuno MaxiSorp 96-well plates
1145 (Nunc, Roskilde,) at 4°C for 4hrs, followed by a blocking step for 1hr using a 5% BSA in
1146 PBST (Tween 20: 0.1%) solution. Synthetic, oligomeric preparations of Aβ1-24 or Aβ1-25
1147 standards or, human TBS and FA brain extracts were incubated at 4°C over-night to allow for
1148 binding to the capture antibody JD1. Detection of Aβ species was achieved using the mouse
1149 monoclonal HRP-conjugated 6E10 (Biolegend) antibody at a dilution of 1:1000. Signals were
1150 measured at an absorbance at 450nm using a Tecan Infinite F500 reader. All samples were
1151 analyzed in triplicates.
1152
1153 **Mouse hippocampal tissue extraction, TMT labelling and LC-MS analysis.**
1154 Mouse hippocampal proteins from PBS control and Aβ oligomer (JD1 positive) treated brain
1155 slices were extracted with 2% SDS (in PBS) containing protease and phosphatase inhibitors
1156 (Roche, Switzerland) followed by centrifugation at 14000 x g for 15min to precipitate any
1157 insoluble material. Prior to proteolysis, samples were cleared of excess SDS using detergent
1158 removal spin columns (Cat# 87777, Pierce, Switzerland) followed by total protein content
1159 normalization using a standard Bradford protein assay. Samples were reduced and alkylated
1160 followed by overnight digestion at 37°C using LysC / Trypsin proteases (Promega) and isobaric
1161 labelling using tandem mass tags (TMT) as described elsewhere. Briefly, the TMT reagent (0.8
1162 mg, Thermo Fisher Scientific) was dissolved in acetonitrile, and 10 µL of the reagent was
1163 added to 30 µL of peptides along with anhydrous ACN to give a final concentration of 30%
1164 v/v. The peptides were then pooled after incubating at room temperature for 1h followed by
1165 C18 stage tip clearing and drying in a speed vacuum.
1166 For Off-gel fractionation, samples were suspended in a 4M urea buffer containing ampholytes
1167 and subjected to off-gel IEF fractionation using a 24 well strip (pH 3-10) (Agilent, 3100 Off-
1168 gel fractionator). Following IEF, fractions were recovered and samples were cleared with C18
1169 stage tips followed by speed vacuum drying and storage at -20°C until LC-MS analysis.
1170

**LC-MS/MS analysis**

Mass spectrometry (MS) analysis was performed on an Orbitrap Exploris 480 mass spectrometer (Thermo Fisher Scientific) coupled to a nano-UPLC Dionex pump. For liquid chromatography (LC) MS/MS analysis, trypsin / LysC digested samples were resuspended in 30-60ul of a mobile phase A solution (2% ACN / water, 0.1% formic acic) and then separated by reversed-phase chromatography using a Dionex Ultimate 3000 RSLC nanoUPLC system on a home-made 75 µm ID × 50 cm C18 capillary column (Reprosil-Pur AQ 120 Å, 1.9 µm) in-line connected with the MS instrument. Peptides were separated by applying a non-linear 150min gradient ranging from 99% solvent A (2% ACN and 0.1% FA) to 90% solvent B (90% ACN and 0.1%FA) at a flow rate of 250nl/min. Full-scan MS spectra (300−1500 m/z) were acquired at a resolution of 120'000 at 200 m/z. Data-dependent MS/MS spectra were recorded followed by HCD (higher-energy collision dissociation) fragmentation on the ten most intense signals per cycle (2 s), using an isolation window of 1.4 m/z. HCD spectra were acquired at a resolution of 60'000 using a normalized collision energy of 32 and a maximum injection time of 100 ms. The automatic gain control (AGC) was set to 100'000 ions. Charge state screening was enabled such that unassigned and charge states higher than six were rejected. Precursors intensity threshold was set at 5'000. Precursor masses previously selected for MS/MS measurement were excluded from further selection for a duration of 20 s, and the mass exclusion window was set at 10 ppm. Theoretical isotopic envelopes of Aβ peptides were drawn using the isotope calculator tool in Data Explorer Software (version 4.9). The mass spectrometry data generated from this study have been deposited to the ProteomeXchange Consortium (http://www.proteomexchange.org) via PRIDE partner repository with the dataset identifier: PXD033934 (10.6019/PXD033934).

**Targeted and quantitative MS analyses**

Parallel reaction montitoring (PRM) analyses were performed as reported earlier (Sathe et al) using an Orbitrap Exploris 480 mass spectrometer (Thermo Fisher Scientific) coupled to a nano-UPLC Dionex pump. Peptides from selected target proteins, SST, NEUG, SYUA were monitored using a targeted inclusion list. The parameters used for the PRM analysis were set as follows: Orbitrap resolution of 35,000, AGC target value of 5 x 10 5, injection time of 200 ms. A precursor target isolation window of 2 m/z was applied and a normalized collision energy

1205 of 35 was employed for MS/MS fragmentation. The PRM method was carried out in an
1206 unscheduled mode and samples were analysed in duplicates. PRM data were analyzed using
1207 the Skyline software package (MacCoss Lab). Acquired raw files were uploaded to Skyline and
1208 peak integration was verified manually.
1209
1210 **MS raw data processing and database searches**
1211 PEAKS Studio X+ Pro (Bioinformatics Solutions Inc.) software was used for data processing.
1212 The raw MS data files were imported into PEAKS Studio software using the following
1213 parameters for the database search: For protein identification the UniProt / Swiss-Prot mus
1214 musculus database (ID: UP000000589) combined with a decoy database was used. For peptide
1215 identification the following settings were used: Enzyme: Trypsin, missed cleavages: 2 precursor
1216 mass tolerance: 10 ppm, fragment mass tolerance: 0.2 Da, minimum charge: 2, maximum
1217 charge: 5, fixed modifications: Carbamidomethyl (C), variable modifications: Oxidation (M),
1218 phosphorylation (STY). False discovery rate (FDR) was calculated based on the target/decoy
1219 database and peptides as well as proteins with FDR threshold of $\leq$ 1% were chosen as true
1220 positive hits.
1221 MaxQuant searches: Label-free and TMT-labelled mouse brain proteomes were processed by
1222 MaxQuant as reported earlier (Tyanova 2016). Briefly, MS raw files were processed using the
1223 peptide identification algorithm of the Maxquant software (ver. 1.5.3.12) using the Andromega
1224 search engine. TMT correction factors were updated according to the values provided
1225 manufacture. MS/MS searches were performed with the following parameters: Peptides had
1226 to have a minimum length of six amino acids to be considered for identification.
1227 Carbamidomethylation was set as a fixed modification, while oxidation of methionine and
1228 protein N-terminal acetylation were set as variable modifications. The enzyme specificity was
1229 set to trypsin and allowed up to two miscleavages. The UniProt / Swiss-Prot mus musculus
1230 database (ID: UP000000589) combined with a decoy database was used. A false discovery rate
1231 (FDR) of $\leq$1% was applied at the proteins and peptide level.
1232 Quantitative data analysis was performed using Skyline (version 21.1.0.278, MacCoss lab,
1233 Uni. Washington, USA), an open source software tool application for quantitative data
1234 processing and proteomic analysis. All integrated peaks were manually inspected to ensure
1235 correct peak detection and integration.
1236 Bioinformatic analysis was carried out using the Perseus (v.1.6.15.0) software environment and
1237 compared with the bioinformatics output generated with the PEAKS Studio X+ Pro software to
1238 identify any putative discrepancies due to the analytical stringencies or search engine

1239 algorithms used in both workflows. Volcano plots were generated using the -log10 of the p-
1240 value on the y-axis versus the mean fold-difference of the log2 transformed quantitative data
1241 on the x-axis. A paired t-test with 'Benjamini-Hochberg FDR' method was applied for multiple
1242 hypothesis corrections. Significance curves in the volcano plot corresponded to an S0 value of
1243 0.5 and an FDR cut-off of 0.05. Protein interaction networks were analyzed and plotted using
1244 the open source platforms: STRING DB (http://string-db.org) (Jensen et al.) and Cytoscape
1245 (v.3.9.0) software (Shannon et al).
1246
1247 **SDS-PAGE and Immunoblotting.**
1248 Where indicated in the results, samples were mixed using either standard SDS Lämmli sample
1249 buffer and heated at 80°C for 5 min prior to loading onto gels (Novex Nupage 4-12% Bis-Tris
1250 gels, 1mm, 15 well, Invitrogen) and ran with Novex Nupage MES-SDS buffer. PAGE
1251 separated samples were electroblotted using a constant voltage of 30V (90min) onto
1252 nitrocellulose (0.22µm) membranes. Following transfer, membranes were boiled in PBS for
1253 2min in a microwave oven (800W) and then blocked for 1h at room temperature under constant
1254 rocking using Odyssey blocking buffer (Li-COR Biosciences, Bad Homburg, Germany)
1255 diluted 1:3 in PBS. Following blocking, membranes were incubated at 4 °C with constant
1256 rocking overnight using the commercially available mouse monoclonal antibodies 6E10 and
1257 4G8 (0.5µg /ml) (Enzo, Life Sciences, Switzerland). Membranes were washed four times with
1258 PBS-Tween (PBS containing 0.1% Tween 20), followed by incubation with a goat anti-rabbit
1259 or anti-mouse secondary IgG antibody (highly cross-adsorbed) (dilution, 1:5000) conjugated
1260 to Alexa Fluor 680 or 800 and scanned in a Li-COR scanner at a wavelength of 700 nm and
1261 800 nm respectively. Densitometric analysis of WB band intensities was carried out using
1262 image J software v.1.43 (NIH).
1263
1264
1265
1266 **Dot blotting**.
1267 Typically, 1ul samples were spotted onto a nitrocellulose membrane, which corresponded to a
1268 total peptide load of 25ng (Aβ1-40) and (AB1-42) unless otherwise stated in the Fig.ures.
1269 Samples were left to dry for 15min followed by blocking of the membrane (30min) with 5%
1270 BSA in PBS solution. Membrane strips were incubated with primary antibodies overnight at
1271 4°C on a shaker. For JD1 probing, membranes were incubated 2-4hrs at RT or over-night at
1272 4°C followed by revelation with a goat anti-mouse, secondary Alexa-flour conjugated

1273 antibody. Neo-epitope antibodies N3, N4, N5s N5ns and N5NH2 were applied as described
1274 earlier (12). Identical solutions and revelation procedures with secondary antibodies were used
1275 as described for immunoblotting above.
1276
1277 **Immunoprecipitation of Tg mouse and human brain tissue.**
1278 Tg mouse (9-12 months) (Tg2576) and cortical human post-mortem brain tissue samples were
1279 extracted using either TBS, 1% SDS (in TBS) or formic acid (70-90%FA) as reported earlier
1280 Rudinskiy et al. (12) Briefly, tissue samples were homogenized (20 strokes on ice) in TBS with
1281 protease inhibitors (Roche, Switzerland) using a Teflon homogenizer. Samples were then
1282 subjected to centrifugation (150,000g) during 45min and supernatant was recovered as the TBS
1283 soluble fraction. Protein pellets were subjected to an additional extraction using either SDS
1284 (1%) or FA (70%) followed by centrifugation. Typically, pellets were extracted with 70-90%
1285 FA overnight at 4°C (to minimize formylation adducts) followed by centrifugation. SDS
1286 fractions were diluted to ≤0.1% SDS final concentration and FA fractions were neutralized to
1287 pH 7.5 with 5M sodium hydroxide (NaOH) solution prior to IP. All samples were initially
1288 depleted of endogenous IgG's using a mixture of protein A&G agarose beads (Roche AG,
1289 Switzerland). Typically, 3-5ug/ml rabbit polyclonal antibody (N3, N4, N5ns & N5NH2),
1290 5ug/ml of JD1 (IgG) or 3-5ug/ml of 6E10 or 4G8 mouse monoclonal was used for IP overnight
1291 under continues rotation (4rpm/min) at 4°C. Samples were eluted with 40% ACN /$H_2O$ & 0.1%
1292 TFA for downstream MS analysis and dried in a speed vacuum or, boiled in Lämmli buffer for
1293 WB analysis. IP'ed samples were either directly analysed by WB or MALDI-TOF/TOF or
1294 further digested overnight using LysN proteolysis prior to LC-MS/MS analysis as outlined
1295 above.
1296
1297
1298
1299
1300 **Animals**
1301 Hippocampal slices were prepared from 8 to 10 week old c57/black 6 mice (c57BL6), obtained
1302 from Charles River UK. Mice were housed in the biomedical facility, University College
1303 Dublin with a 12 h light/dark cycle with food and water ad libitum. All experiments were
1304 conducted under license from the Dept. of Health, Ireland, Directive 63/2010/EU.
1305
1306 **Hippocampal Slices**

1307 Parasagittal hippocampal slices, were prepared using a vibrotome (Leica VT1000S) as
1308 described previously (62,63) using ice cold cutting solution (mM) NaCl 87; $NaHCO_3$ 25;
1309 Glucose 25; Sucrose 75; KCl 2.5; $NaH_2PO_4$ 1.25; $CaCl_2$ 0.5; $MgSO_4$ 7; bubbled with 95%
1310 $O_2$/5% $CO_2$ (carbogen). Slices (400-µm thick) were transferred to a holding chamber
1311 containing aCSF (mM) NaCl 119; $NaHCO_3$ 26.2; Glucose 11 mM; KCl 2.5; $NaH_2PO_4$ 1; $CaCl$
1312 $_2$ 2.5; $MgSO_4$ 1(also used for recording); bubbled with carbogen and were allowed to recover
1313 at room temperature for at least 90 min Slices were transferred to a recording chamber, secured
1314 by means of a harp with fine nylon strings and perfused with recording aCSF at a rate of
1315 5 ml/min maintained at 28–30 °C for the duration of all experiments. A horizontal puller (DMZ
1316 universal puller, Germany) was used to makerecording electrodes from borosilicate capillary
1317 glass (GC150 F-10, Havard apparatus), Electrodes (2–5 MΩ) were filled with recording aCSF.
1318 The Shaffer-collateral pathway was stimulated using a mono-polar electrode (FHC, Bowdoin,
1319 USA) at 0.033 Hz (duration: 100 µs), the return electrode was a silver/silver chloride wire
1320 placed in the recording bath. Extracellular field excitatory post synaptic potentials (fEPSPs)
1321 were recorded in the $CA_1$ *stratum radiatum* and paired stimuli were delivered with an inter-
1322 stimulus interval of 50 ms in order to monitor paired pulse facilitation (PPF). The voltage
1323 signal was filtered at 5 kHz and stored for off-line analysis using a personal computer
1324 interfaced with a Digidata 1440 and pclamp 10. Signals were amplified by a HS2A headstage
1325 (Molecular Devices, USA) connected to an Axoclamp 2B system (Molecular Devices, USA)
1326 and a Brownlee 410 Precision preamplifier. The stimulus voltage was adjusted to evoke a
1327 fEPSP that was 40–50% of the maximal response (maximum fEPSP just prior to the formation
1328 of a spike caused by cell firing) for the duration of all experiments. When a stable baseline had
1329 been recorded for 20 min a Master 8 (AMPI) timer was used to deliver two trains of high
1330 frequency stimuli (HFS), 100 Hz for 1 s, with an inter-train interval of 30 s. Following the
1331 application of HFS, the synaptic response was recorded for a further period of 60 min. All
1332 results are presented as mean ± SEM. The "*n*" numbers quoted refer to the number of slices
1333 used. Control and test experiments in a given section were conducted on the same day on slices
1334 from the same animal.
1335
1336 **Development of monoclonal antibody against LMW Aβ oligomers.**
1337 Briefly, mice were immunized with the linear sequence of Aβ1-24 (CONH2) as well as an
1338 aggregated form of Aβ1-24 peptide. Eight weeks following immunization, sera were tested by
1339 ELISA for antibodies against fresh (linear) and oligomeric Aβ species. Mice testing positive
1340 for anti-Aβ antibodies were then given booster injections of 50 ug of an oligomeric form of

1341 Aβ1-25. IgM type antibodies consisted of the predominantly identified type of anti-Aβ
1342 antibodies found following this protocol. Antibody type switching and grafting from IgM to
1343 IgG was then carried using recombinant technologies. All work was carried out by Eurogentec
1344 SA, (Liege, Belgium).
1345
1346 **Immunofluorescence and array tomography imaging of human post-mortem brain tissue.**
1347 Samples from the inferior temporal gyrus of 4 AD patients was prepared for array tomography
1348 as described previously (12,34). Brain samples were obtained with ethical approval via the
1349 University of Edinburgh Sudden Death Brain Bank and the Alzheimer Scotland Brain and
1350 Tissue Bank. This study was reviewed and approved by the Edinburgh Brain Bank ethics
1351 committee and the Academic and Clinical Central Office for Research and Development, a
1352 joint office of the University of Edinburgh and NHS Lothian (approval number 15-HV-
1353 016). The Edinburgh Brain Bank is a Medical Research Council funded facility with
1354 research ethics committee (REC) approval (16/ES/0084). Briefly, tissue was collected at
1355 autopsy, fixed for 3 hours in 4% paraformaldehyde with 2.5% sucrose, dehydrated through a
1356 series of ethanols, and embedded in LR White resin. Ribbons of 70nm serial sections were cut
1357 with an ultracut microtome (Leica). Ribbons were stained with, primary antibodies OC (Sigma
1358 AB2286, 1:200), JD1 (IgG, 1:200), and PSD95 (Synaptic Systems 124 014; 1:50) and detected
1359 with anti-mouse IgG alexa fluor 594, and anti-rabbit alexa fluor 405, and anti-guinea pig alexa
1360 fluor 647 (all at 1:50). Images from 5 serial sections were acquired on a Leica TSC SP8 confocal
1361 with a 63x oil objective. Individual images were made into stacks, aligned, and segmented with
1362 custom software that can be found at https://github.com/Spires-Jones-Lab For
1363 immunofluorescence staining of 4 µm paraffin sections from formalin fixed tissue, sections
1364 were de-waxed, rehydrated, and stained with amyloid beta antibodies JD1 (1:500) and OC
1365 (1:1000) and secondaries donkey anti-rabbit 647 and donkey anti-mouse 594. Thioflavin S
1366 counterstain was used to label fibrils (0.01%). Image stacks were acquired on a Leica TSC SP8
1367 confocal with a 63x objective.
1368
1369 **Transmission Electron Microscopy (TEM).**
1370 Aβ peptide (5µl) samples were deposited on Formvar-coated 200-mesh copper grids (Electron
1371 Microscopy Sciences, Hatfield, PA). Grids were washed with two drops of double-distilled
1372 $H_2O$ and stained with two drops of freshly prepared 1% (w/v) uranyl formate (Electron
1373 Microscopy Sciences). The samples were analysed at room temperature using a Tecnai Spirit

(FEI, The Netherlands) electron microscope equipped with a LaB6 filament and operated at an acceleration voltage of 80 kV. Images were recorded with an Eagle (FEI, The Netherlands) camera 4098 X 4098 pixels. Representative images of the main Aβ structures were taken at different magnifications ranging from 30kX to 50kX.

**C. elegans strain**

C. elegans overexpressing Aβ42 peptide were developed as reported before (24). Briefly, c. elegans were cultured at 20 °C on nematode growth medium (NGM) agar plates seeded with E. coli strain OP50 unless stated otherwise. The GMC101 strain was used in this study and was provided by the Caenorhabditis Genetics Center (University of Minnesota).